
Article:
Douglas, KM orcid.org/0000-0002-3281-3685, Blitz, MA, Feng, W orcid.org/0000-0002-9907-9120 et al. (4 more authors) (2019) Low temperature studies of the rate coefficients and branching ratios of reactive loss vs quenching for the reactions of $^1CH_2$ with C_2H_6, C_2H_4, C_2H_2. Icarus, 321. pp. 752-766. ISSN 0019-1035

https://doi.org/10.1016/j.icarus.2018.12.027

Low temperature studies of the rate coefficients and branching ratios of reactive loss vs quenching for the reactions of $^1CH_2$ with C_2H_6, C_2H_4, C_2H_2

Kevin M. Douglas[a*], Mark A. Blitz[a,b], Wuhu Feng[a,b], Dwayne E. Heard[a,b], John M.C. Plane[a,b], Haneef Rashid[a], and Paul W. Seakins[a,b*]

[a]School of Chemistry, University of Leeds, Leeds, LS2 9JT, UK

[b]National Centre for Atmospheric Science (NCAS), University of Leeds, Leeds, LS2 9JT, UK

Abstract

The kinetics of the reactions of the first excited state of methylene, $^1CH_2$, with C_2H_2, C_2H_4, and C_2H_6, have been measured over the temperature range 43 – 298 K by pulsed laser photolysis, monitoring $^1CH_2$ removal by laser induced fluorescence. Low temperatures were obtained using a pulsed Laval expansion (43 – 134 K), while a slow flow reaction cell was used for temperatures of 160 K and above. The rate coefficients for the reactions with C_2H_2, C_2H_4, and C_2H_6, all showed a strong negative temperature dependence. In combination with other literature data, the coefficients can be parameterized as:

$$k_{C_2H_2}(43 \leq T/K \leq 298) = (3.22 \pm 0.15) \times 10^{-10} \times (T/298)^{(-0.394 \pm 0.066)}$$

$$k_{C_2H_4}(43 \leq T/K \leq 298) = (2.16 \pm 0.14) \times 10^{-10} \times (T/298)^{(-0.612 \pm 0.089)}$$

$$k_{C_2H_6}(43 \leq T/K \leq 298) = (1.78 \pm 0.10) \times 10^{-10} \times (T/298)^{(-0.545 \pm 0.078)}$$

Branching ratios for reactive removal of $^1CH_2$ vs quenching to ground state were also determined for all three colliders and for H_2 and CH_4, at temperatures between 100 and 298 K. The values measured show that the dominant removal process of $^1CH_2$ by H_2, C_2H_2, and C_2H_4, changes from reactive removal to quenching to ground state $^3CH_2$ as the temperature decreases from 298 K to 100 K, while for CH_4 and C_2H_6, reactive removal drops from around 85 % to around 55 %. The impacts of the new measurements for Titan's atmosphere are examined using a 1D chemistry and transport model. A significant increase (~25%) in the mixing ratio of benzene between 500 and 1550 km is calculated, due to the increased production of C_3H_3 from the reaction of $^1CH_2$ with C_2H_2.

1. Introduction

The photolysis of methane by UV photons is the primary source of hydrocarbon radicals in the atmospheres of Titan and the giant planets. Although there is still significant uncertainty in the branching ratios of products as a function of wavelength (Blitz and Seakins, 2012; Romanzin et al., 2005), the production of the first excited state of methylene ($^1CH_2$ a^1A_1) is a significant channel (48 ± 5 %) at the dominant Lyman-α (121.6nm) wavelength (Gans et al., 2011):

$$CH_4 + h\nu \rightarrow {}^1CH_2 + H_2 \qquad (R1)$$

The photolysis of methyl radicals, CH_3, is a further source of $^1CH_2$.

$$CH_3 + hv \rightarrow {}^1CH_2 + H \quad \text{(R2)}$$

$^1CH_2$ is a reactive species that is able to insert into chemical bonds to form chemically activated intermediates that rapidly fall apart (e.g. R3a and R4a).

$$^1CH_2 + H_2 \rightarrow CH_4^* \rightarrow CH_3 + H \quad \text{(R3a)}$$

$$^1CH_2 + CH_4 \rightarrow C_2H_6^* \rightarrow 2\ CH_3 \quad \text{(R4a)}$$

In competition with chemical reaction, collisions of $^1CH_2$ can result in electronic relaxation down to the ground triplet state of methylene ($^3CH_2$ X^3B_1):

$$^1CH_2 + H_2 \rightarrow {}^3CH_2 + H_2 \quad \text{(R3b)}$$

$$^1CH_2 + CH_4 \rightarrow {}^3CH_2 + CH_4 \quad \text{(R4b)}$$

Despite the small energy gap between the ground and first excited states of methylene (37.7 kJ mol^{-1} (Jensen and Bunker, 1988)), the two states have a markedly different reactivity. Unlike the singlet, the triplet is relatively unreactive with closed shell species, generally reacting several orders of magnitude slower than singlet methylene. Instead, the major loss process of $^3CH_2$ on Titan are reactions with radical species such as H (R5) and CH_3 (R6):

$$^3CH_2 + H \rightarrow CH + H_2 \quad \text{(R5)}$$

$$^3CH_2 + CH_3 \rightarrow C_2H_4 + H \quad \text{(R6)}$$

This competition between reaction and relaxation of $^1CH_2$ is also observed in reactions with acetylene (R7), ethylene (R8), and ethane (R9):

$$^1CH_2 + C_2H_2 \rightarrow C_3H_4^* \rightarrow C_3H_3 + H \quad \text{(R7a)}$$

$$^1CH_2 + C_2H_2 \rightarrow {}^3CH_2 + C_2H_2 \quad \text{(R7b)}$$

$$^1CH_2 + C_2H_4 \rightarrow C_3H_6^* \rightarrow C_3H_5 + H \quad \text{(R8a)}$$

$$^1CH_2 + C_2H_4 \rightarrow {}^3CH_2 + C_2H_4 \quad \text{(R8b)}$$

$$^1CH_2 + C_2H_6 \rightarrow C_3H_8^* \rightarrow C_2H_5 + CH_3 \quad \text{(R9a)}$$

$$^1CH_2 + C_2H_6 \rightarrow {}^3CH_2 + C_2H_6 \quad \text{(R9b)}$$

The formation of the propargyl radical (C_3H_3) from Reaction 7a is of particular importance, as it has been proposed as an important radical route to benzene (C_6H_6) formation on Titan (via R10) (Wilson and Atreya, 2003). Observed benzene mixing ratios on Titan (Cui et al., 2009; Magee et al., 2009) are often significantly higher than those predicted by photochemical models (Hebrard et al., 2013). Benzene is also believed to be an important first step in the formation of polyaromatic hydrocarbons and photochemical aerosols (Lorenz, 2014; Yoon et al., 2014) that are responsible for the detached haze layer observed between altitudes of around 300 – 500 km, and recently benzene ice clouds have been detected in the lower stratosphere of Titan (Vinatier et al., 2018). Reaction 5 is an important source of methylidene (CH) radicals; the primary loss of CH on Titan is via reaction with methane (R11), leading to the formation of unsaturated species such as ethylene and acetylene (R12) (Blitz et al., 1997; Canosa et al., 1997; Thiesemann et al., 1997):

$$2\ C_3H_3 + M \rightarrow C_6H_6 + M \quad \text{(R10)}$$

$$CH + CH_4 \rightarrow C_2H_4 + H \quad \text{(R11)}$$

$$C_2H_4 + h\nu \rightarrow C_2H_2 + 2H \quad \text{(R12)}$$

Therefore both methylene species are important to different aspects of Titan's complex photochemistry.

Methane photolysis is also the major source of hydrocarbons radicals in the atmospheres of the giant planets. However, in these environments, $^1CH_2$ chemistry is dominated by the reaction with molecular hydrogen (R3) (Gannon et al., 2008; Hancock and Heal, 1992; Wagener, 1990).

Measurements indicate that relaxation accounts for only ~ 15 % of the overall loss process for reactions of $^1CH_2$ with H_2, CH_4, C_2H_2, C_2H_4, and C_2H_6, at around 300 K (Gannon et al., 2010a; Gannon et al., 2010b; Gannon et al., 2008). In a previous publication, we reported the branching ratio (BR) between electronic relaxation and chemical reaction as a function of temperature down to 73 K for the reaction of $^1CH_2$ with H_2 (R3) and CH_4 (R4) (Douglas et al., 2018), indicating that by 73 K relaxation had risen to become the dominant removal process, accounting for ~ 70 % of $^1CH_2$ loss. BRs for the reaction of $^1CH_2$ with C_2H_2 (R7) and C_2H_4 (R8) have also been measured in this laboratory as function of temperature between 195 and 498 K (Gannon et al., 2010a; Gannon et al., 2010b; Gannon et al., 2008), and indicate that the fraction of reactive loss decreases from ~ 85 % at 300 K, down to ~ 30 % at 195 K. These results suggest that at the temperatures of Titan's photochemically active thermosphere (120 – 160 K), in reactions of $^1CH_2$ with acetylene and ethylene, relaxation to $^3CH_2$ should be the dominant process, however no direct measurements at these temperatures have been made. For the reaction of $^1CH_2$ with ethane, there are currently no temperature dependant BR measurements.

Cui et al. (2009) reported that at 1050 km, ~96.6 % of Titan's atmosphere is N_2, with CH_4 and H_2 accounting for ~3.0 and ~0.4 % respectively. In the reactions of $^1CH_2$ with non-reactive species such as N_2 and He, relaxation is the only possible loss process:

$$^1CH_2 + N_2 \rightarrow {}^3CH_2 + N_2 \quad \text{(R13)}$$

$$^1CH_2 + He \rightarrow {}^3CH_2 + He \quad \text{(R14)}$$

In a previous publication, we reported a sharp upturn in the removal of $^1CH_2$ by N_2 (R13) at temperatures below ~ 160 K (Douglas et al., 2018), and indicated that this, in conjunction with the enhancement of reactions R3a and R4a at low temperatures, would result in a reduced steady state concentration of $^1CH_2$, and enhanced production of $^3CH_2$. Current temperature dependant studies of the total removal rates of $^1CH_2$ by C_2H_2, C_2H_4, and C_2H_6, show a modest inverse temperature dependence (Gannon et al., 2010a; Hayes et al., 1996), suggesting that despite a lower steady state concentration of $^1CH_2$, at temperatures relevant to Titan ($\leq$ 180 K), these reactions may still be important. However, at present, there have been no studies investigating removal rates of $^1CH_2$ with these C_2H_x species at temperatures below ~ 200 K.

Photochemical models of Titan's atmosphere deal with methylene chemistry in varying levels of detail. Some models only consider the reactions of $^1CH_2$ with the most abundant species in Titan's atmosphere, namely N_2, CH_4, and H_2 (Krasnopolsky, 2014; Lara et al., 2014; Toublanc et al., 1995). Others that do include reactions of $^1CH_2$ with acetylene, ethylene, and ethane, often fail to account for the temperature dependence of the reactions (Dobrijevic et al., 2016; Hebrard et al., 2007; Lavvas et al., 2008; Willacy et al., 2016), while some ignore the role of relaxation, a minor channel at room temperature (Wilson and Atreya, 2004). The way in which various models treat reactions R7, R8, and R9 is discussed below.

In the present paper, we report rate coefficients for the reactions of $^1CH_2$ with C_2H_2, C_2H_4, and C_2H_6, over a temperature range of 43 – 298 K. Rate coefficients for the reaction of $^3CH_2$ with O_2 over a temperature range of 100 – 298 K are also reported, as despite being of no direct relevance to Titan, this reaction was employed in the determination of branching ratios in this study. In addition, product studies have allowed us to determine the BR between reaction and relaxation for the reactions of $^1CH_2$ with H_2, CH_4, C_2H_2, C_2H_4, and C_2H_6, over a temperature range of 100 – 298 K. The impacts of these new measurements are also explored using a 1D transport model of Titan's atmosphere. The apparatus and experimental procedures employed in this study are outlined in Section 2, and the results discussed in Section 3. The details of the Titan atmospheric model used in this study are given in Section 4, together with the results and implications of the model outputs. Section 4 also discussed the wider implications of our new rate coefficients and BRs for other low temperature astrophysical environments.

2. Experimental Procedure

All studies were carried out using a pulsed laser photolysis-laser induced fluorescence (PLP-LIF) technique, with detection of either the $^1CH_2$ reagent or H atom product. Measurements of rate coefficients and BRs between 45 and 135 K were carried out using a pulsed Laval nozzle apparatus. The use of a Laval nozzle expansion to study low temperature reactions was first demonstrated by Rowe and co-workers, who used the technique to study ion-molecule reactions (Rowe and Marquette, 1987). The technique was later adopted for the study of neutral-neutral reactions by the use of PLP-LIF (Brownsword et al., 1997; Canosa et al., 1997), and has since enjoyed considerable success, and has been extensively reviewed (Sims and Smith, 1995; Smith, 2006; Smith et al., 2006). The pulsed Laval nozzle apparatus employed in this study has been discussed in detail in recent publications (Caravan et al., 2015; Gomez Martin et al., 2014; Shannon et al., 2013; Shannon et al., 2010; Taylor et al., 2008), so only a brief description is given here. The reaction mixture consisting of radical precursor, reagent, and bath gas, was introduced to a 1 cm^3 stainless steel reservoir via two pulsed solenoid valves (Parker 9 series), fired at a 5 Hz repetition frequency with a pulse duration of between 10 and 20 ms, depending on the Laval nozzle employed. The gas mixture was then expanded through the convergent-divergent shaped Laval nozzle into a low pressure stainless steel cylindrical chamber (774 mm length × 240 mm diameter), producing a thermally equilibrated, low temperature jet. The temperature and density profile of the jet were characterized by impact pressure measurements, and the temperature also by

rotationally resolved laser-induced fluorescence spectroscopy. The properties of the characterized expansions used in this study are given in Table 1.

Ketene (CH_2CO), the $^1CH_2$ precursor, was generated by pyrolysis of acetic anhydride (> 99 %, Alfa Aesar) (Fisher et al., 1953), purified by trap-to-trap distillation and diluted in a cylinder with the bath gas (He or N_2), and the purity checked by IR spectroscopy (Arendale and Fletcher, 1957) . Reagent and bath gases used were all of analytical quality (He 99.995 %, N_2 99.9992 %, O_2 99.5 %, H_2 99.99 %, C_2H_2 > 98.5 %, C_2H_4 99.9 %, C_2H_6 > 99 %, all BOC gases). Reaction gas mixtures were obtained by flowing the relevant gases through calibrated mass flow controllers (MFCs) (MKS Instruments) and allowing mixing in a 1 L ballast tank prior to the pulsed solenoid valves. The photolysis laser was introduced collinearly with the axis of the expanded gas flow, to produce a uniform radical density. The probe laser was introduced perpendicularly to photolysis laser beam, and the fluorescence collected via a series of lenses and observed with a channel photomultiplier tube (CMP) (Perkin Elmer C1943 for $^1CH_2$ detection and Perkin Elmer C1911 for H atom detection) mounted at 90º to both laser beams. When detecting fluorescence from $^1CH_2$, the CMP was gated to remove the intense probe laser scatter pulse.

Measurements of rate coefficients and branching ratios at 160 K and above were carried out in a slow-flow reaction cell apparatus. The reaction cell was a six-way stainless steel cross that could be cooled by immersion, either in dry ice to reach 198 K, or a bath of dry ice/ethanol for 160 K. Temperatures around the observation region were monitored using a thermocouple. Preparation of the $^1CH_2$ precursor, ketene, and the reagent and bath gases used, were as detailed above. Reaction gas mixtures were obtained by flowing the relevant gases through calibrated MFCs (MKS Instruments) and combining in a stainless steel transfer line before introduction into the cell. The total flow rate was sufficient to ensure a fresh flow of gas into the cell for each photolysis laser pulse. The total pressure, as measured by two gauges (0 – 10 Torr and 0 – 100 Torr Baratron), was controlled by a valve on the exit line to the pump. The photolysis and probe laser beams were introduced collinearly on opposite sides of the cell, so as to obtain maximum overlap in the observation region. Fluorescence was observed with a channel photomultiplier tube (Perkin Elmer C1943 for $^1CH_2$ detection and Perkin Elmer C1911for H atom detection) mounted at 90º to the laser beams. Again, when detecting fluorescence from $^1CH_2$, the CMP was gated to remove the intense probe laser scatter pulse.

2.1 Rate coefficient measurements

For both experiments, the rate coefficients for the reaction of $^1CH_2$ with co-reactants C_2H_2 (R7), C_2H_4 (R8), and C_2H_6 (R9), were measured by monitoring the temporal decay of the $^1CH_2$ radical via PLP-LIF. The experiments were performed under pseudo-first-order conditions so that the concentration of the co-reagent was in great excess of the $^1CH_2$ concentration. $^1CH_2$ was produced by the pulsed photolysis of ketene (R15) at 308 nm (Lambda Physic LPX100). The photolysis mechanism is well established at this wavelength, with > 95 % of the methylene produced being in the required singlet state (Morgan et al., 1996; Wade et al., 1997). The subsequent decay of $^1CH_2$ due to reaction and other loss

processes was measured by probing the $b^1B_1 \leftarrow a^1A_1$ transition at either ~590.7 nm or ~653.3 nm using light from an excimer pumped dye laser (Lambda Physic LPX100 pumping a Lambda Physik FL3002 with Rhodamine 6G or Rhodamine Special as the dye). The fluorescence was imaged using two lenses and monitored using a photomultiplier tube (PMT) fitted with a 589.5 nm interference filter (Ealing Corp. λ_{max} = 589.6, fwhm = 5 nm) or a 560 nm high pass filter. The temporal evolution of the $^1CH_2$ radicals was recorded by varying the time delay between photolysis and probe lasers, a typical example of which can be seen in Figure 1. At very short times following photolysis, probe laser excitation scans revealed the presence of rotationally excited $^1CH_2^*$, which rapidly relaxes to the temperature of the jet obtained independently by impact pressure measurements (R16).

The reaction scheme for the formation and removal of $^1CH_2$ is given by:

$$CH_2CO + h\nu \rightarrow {}^1CH_2, {}^1CH_2^* + \text{co-products} \qquad \text{(R15)}$$

$$^1CH_2^* \xrightarrow{k_{rel}} {}^1CH_2 \qquad \text{(R16)}$$

$$^1CH_2 + R \xrightarrow{k_r} \text{Products} \qquad \text{(R17)}$$

where $^1CH_2^*$ is an initially rotationally excited singlet methylene radical, formed in v" = 0 from photolysis of the precursor, R is the co-reagent, k_{rel} is the rate coefficient for rotational relaxation of the rotationally excited singlet methylene radical, and k_r is the bimolecular rate coefficient for the reaction of singlet methylene with the co-reagent. As the experiment was carried out under pseudo-first-order conditions ([R] » [$^1CH_2$]), the temporal evolution of $^1CH_2$ is given by:

$$[\,{}^1CH_2]_t = \left(\frac{k_{rel}}{k_{obs}-k_{rel}}\right)[\,{}^1CH_2^*]_0(e^{-k_{rel}.t} - e^{-k_{obs}.t}) + [\,{}^1CH_2]_0 e^{-k_{obs}.t} \qquad \text{(E1)}$$

and

$$k_{obs} = k_r[R] + k_{loss} \qquad \text{(E2)}$$

where k_{obs} is the pseudo-first-order rate constant, t is the time delay between photolysis and probe laser pulses, and k_{loss} is the total rate coefficient for the other minor first order loss processes (diffusion, reaction with the ketene precursor, and relaxation via the buffer gas). Equation E1 was fitted to the $^1CH_2$ profiles to extract the parameters k_{rel}, k_{obs}, $[^1CH_2^*]_0$, and $[^1CH_2]_0$. A plot of k_{obs} vs [R] then gives a straight line of gradient k_r and intercept of k_{loss}. Figure 2 shows an example of such a plot, and the small intercept (relative to the total rate of removal) demonstrates that the reaction with the co-reagent dominates $^1CH_2$ removal.

2.2 Branching ratio measurements

Experiments to determine the BR between relaxation and reaction were carried detecting H atom products, using the same pulsed Laval nozzle and reaction cell apparatus described above. The H atom signal was monitored by LIF at the Lyman-α transition (~ 121.6 nm). Lyman-α radiation was generated by focusing the frequency doubled output (~364.8 nm) of a Nd:YAG pumped dye laser (Litron LYP 664-10 pumping a Sirah Cobra Stretch) into a frequency tripling cell containing a krypton/argon mix (~1 : 2.5) at ~ 500 Torr (Mahon

et al., 1979). The resonant fluorescence was imaged using two lenses and monitored using a solar blind CMP (Perkin Elmer 1911). The temporal evolution of the H atom signal was recorded by varying the time delay between the photolysis and probe lasers, typical examples of which can be seen in Figures 3-5. To account for the attenuation of the Lyman-α radiation by the substrate gases, the probe laser intensity was monitored using a PMT (Thorn EMI, solar blind with a 121 nm VUV interference filter, Acton Optics) mounted equidistant from the reaction zone, and the output used to normalise the fluorescence signal on a shot-by-shot basis. In this manner, any fluctuations in probe laser power were also corrected for.

In a previous paper the BRs for the reaction of $^1CH_2$ with H_2 and CH_4 were determined by monitoring the production of OH from the reaction of ground state $^3CH_2$ with O_2 (R19) (Douglas et al., 2018). However due to the efficient quenching of higher vibrational states of OH by C_2H_2, C_2H_4, and C_2H_6, we could not use this method to determine BRs for these larger hydrocarbons. Instead, the production of H atoms from reaction (R19) was monitored and the BRs determined using a similar scheme as before. This scheme is summarised in Figure 3. Pairs of experiments were conducted in which any $^3CH_2$ produced from the relaxation of $^1CH_2$ was titrated with O_2 to produce H atoms, and the amount of H atoms produced monitored both with and without the reactive co-reagents present. For experiments without the reactive co-reagent present, all $^1CH_2$ produced following the pulsed photolysis of ketene would be electronically relaxed to $^3CH_2$ via reaction R18, and by collisions with the bath gas (either N_2 (R13), or He (R14)).

$$^1CH_2 + O_2 \rightarrow {}^3CH_2 + O_2 \qquad \text{(R18)}$$

For the reaction between $^1CH_2$ and O_2, relaxation has been shown to be the only loss process on timescales applicable to this work (Blitz et al., 2003; Hancock and Haverd, 2003). This is reasonably assumed to be the case over the temperature range employed in this study, as evidenced by the fact that the removal rate of $^1CH_2$ with O_2 over the temperature range of 43 – 298 K (Douglas et al., 2018), remains over an order of magnitude faster than the H atom production rates observed in this study (Table II). Following relaxation of $^1CH_2$ to $^3CH_2$, the slow growth of H atoms from R19 was then monitored:

$$^3CH_2 + O_2 \xrightarrow{k_{\text{growth}}} \text{H + products} \qquad \text{(R19)}$$

A second experiment was then carried out, in which the reactive co-reagent is present. In this case, some of the $^1CH_2$ produced following flash photolysis of ketene may be removed by reaction rather than relaxation, resulting in less $^3CH_2$ production and a smaller amount of H atoms produced following titration with O_2.

The experimental conditions employed in determining BRs were such that the initial relaxation or removal of $^1CH_2$ could be considered to take place instantaneously when compared with the slow growth and subsequent loss of H atoms. Pseudo-first-order conditions were also met, such that $[O_2] \gg [^3CH_2]$. Thus the temporal evolution of the H atoms can be approximated by:

$$[\mathrm{H}]_t = \left(\frac{k_{\text{growth}}}{k_{\text{removal}} - k_{\text{growth}}}\right)[\,{}^1\mathrm{CH}_2]_{rel}\left(e^{-k_{\text{growth}}\cdot t} - e^{-k_{\text{removal}}\cdot t}\right) \qquad \text{(E3)}$$

where k_{growth} is the pseudo-first-order rate coefficient for the reaction between $^3CH_2$ and O_2, $[^1CH_2]_{rel}$ is the amount of $^1CH_2$ removed by relaxation (and thus the amount of $^3CH_2$ produced by relaxation), and $k_{removal}$ is the total rate coefficient for first order loss processes of H atoms (diffusion and reaction with the ketene precursor and reactive co-reactant). Thus, by monitoring the H atom growth and loss, the amount of $^3CH_2$ initially produced via relaxation of $^1CH_2$ can be determined, and by comparing this value with and without the reactive co-reagent present, the amount of $^1CH_2$ being removed by reaction when the reactive co-reagent is present can be determined.

An additional complication with this scheme arises when measuring BRs for H_2, C_2H_2, and C_2H_4, as H atoms are also produced directly from the reactive channel of $^1CH_2$ with these species (R3a, R7a, and R8a). However as stated above, the H atoms produced via this direct channel are formed on significantly shorter timescale than those formed via R19 (~ 200 times faster), and so can be considered as an instantaneous H atom signal. Under these conditions, the temporal evolution of the H atom signal can be approximated by equation 4:

$$[\mathrm{H}]_t = \left(\frac{k_{\mathrm{growth}}}{k_{\mathrm{removal}} - k_{\mathrm{growth}}}\right)[\,^3\mathrm{CH}_2]_0\left(e^{-k_{\mathrm{growth}}.t} - e^{-k_{\mathrm{removal}}.t}\right) + [\mathrm{H}]_0 e^{-k_{\mathrm{removal}}.t} \quad \text{(E4)}$$

where $[H]_0$ is the instant H atom signal, produced via the reactive removal of $^1CH_2$ by reactions R3a, R7a, and R8a. Thus the BR can again be obtained by monitoring the H atom signal both with and without the reactive co-reagent present. By monitoring the temporal evolution of the H atom signal, the amount of $^3CH_2$ initially produced via relaxation of $^1CH_2$ by H_2, C_2H_2, and C_2H_4 can be determined, and by comparison of this value to the amount of $^3CH_2$ produced with no reactive species is present, the amount of $^1CH_2$ removed chemically by H_2, C_2H_2, and C_2H_4 can be determined. It should be noted that in these experiments, 'instant' H atom signal was only observed when the H_2, C_2H_2, or C_2H_4 reagent was present, indicating that no H atoms are produced by the direct 308 nm photolysis of ketene. This is expected as the HCCO + H channel is thermodynamically inaccessible following 308 nm photolysis of ketene. In practice, measuring BRs for C_2H_2 and C_2H_4 using this scheme proved difficult, as in order to measure accurate BRs, in the experiment with the reactive co-regent R is present, the majority of $^1CH_2$ must be removed by R rather than the bath gas and O_2, putting constraints on the concentrations of C_2H_2 and C_2H_4 required. Attenuation of the ~ 121.6 nm probe laser and H atom fluorescence at these concentrations of C_2H_2 and C_2H_4 then made such experiments untenable. This was not a problem for H_2, which does not attenuate light at ~ 121.6 nm. Instead, BRs for C_2H_2 and C_2H_4 were determined by comparing the direct H atom production from the reactive channel of $^1CH_2$ with these species to that of a calibration reaction as described below.

When measuring BRs for H_2 using the above scheme, for completeness a third experiment was also carried out, in which no O_2 was present. This allowed the (effectively) instant H atom signal produced via Reaction 3a to be determined, allowing the parameter $[H]_0$ in equation 4 to be fixed when analysing the H atom trace obtained with O_2 and H_2 present. An example of all three H atom traces used in the determination of BRs for H_2 can be seen in Figure 4.

To determine BRs for the reaction of $^1CH_2$ with C_2H_2 and C_2H_4, experiments were carried out in which the direct H atom signal from reaction R7a or R8a was monitored, and then compared to the direct H atom signal from a calibration reaction; a reaction of $^1CH_2$ with a species that generates a known fraction of H atoms. Having determined the BR for production of H atoms from the reaction of $^1CH_2$ with H_2 (R3a) in this study and a previous study (Douglas et al., 2018), this reaction was chosen as the calibration reaction. An example of a comparison between the H atom signal obtained from the reaction or $^1CH_2$ with C_2H_2 and the calibrant (H_2) can be seen in Figure 5. Pseudo-first-order conditions were met, such that $[C_2H_2]$, $[C_2H_4]$, and $[H_2]$ » $[^1CH_2]$. Thus the temporal evolution of the H atom signal in these experiments can be approximated by:

$$[\mathrm{H}]_t = \left(\frac{k_{\mathrm{growth}}}{k_{\mathrm{removal}} - k_{\mathrm{growth}}}\right) Yield_{\mathrm{H}} [\,^1\mathrm{CH}_2]_0 \left(e^{-k_{\mathrm{growth}} \cdot t} - e^{-k_{\mathrm{removal}} \cdot t}\right) \qquad \text{(E5)}$$

where k_{growth} is the pseudo-first-order rate coefficient for the reaction between $^1CH_2$ and C_2H_2, C_2H_4, and H_2, $[^1CH_2]_0$ is the initial amount of $^1CH_2$ generated by the photolysis of ketene (a constant). $Yield_H$ is the H atom yield from the reaction of $^1CH_2$ with C_2H_2 or C_2H_4 in comparison to that from the calibration reaction (set as 1), and $k_{removal}$ is the total rate coefficient for first order loss processes of H atoms (diffusion and reaction with the ketene precursor and reactive co-reactants). To aid analysis of the relative H atom yields, conditions employed were such that for each pair of experiments carried out, the growth rate of H atoms from reactions R7a or R8a, and from the calibration reaction (R3a) were the same. As described below, the H atom LIF signals were also corrected for absorption of the Lyman-α radiation by the substrate gases.

In addition to measuring BRs, when monitoring H atom product from the reaction of $^1CH_2$ with H_2, C_2H_2, and C_2H_4, some kinetic traces were also collected to confirm that the H atoms were produced with the same pseudo-first order rate coefficient with which $^1CH_2$ was removed. The pseudo-first order rate constants obtained were identical, within experimental error. Experiments were also carried out to determine the rate coefficient for the reaction of $^3CH_2$ with O_2 (R19), by monitoring the H atom growth from the reaction as a function of $[O_2]$.

3. Results

3.1. Kinetics

An example of the temporal evolution of the $^1CH_2$ LIF signal following 308 nm photolysis of ketene in the presence of a co-reactant, C_2H_2, is shown in Figure 1. Figure 2 gives an example of a bi-molecular plot, formed by plotting k_{obs} with varying co-reactant concentration $[C_2H_4]$, the gradient of which yields the bimolecular rate coefficient. The bimolecular rate coefficients for the reaction of $^1CH_2$ with C_2H_2, C_2H_4, and C_2H_6, and for the reaction of $^3CH_2$ with O_2, are presented in Table 2 and compared with other literature data in Figures 6 and 7. The errors reported in this work are statistical at the 2σ level. For each temperature and co-reactant, bimolecular rate coefficients were measured at three or more different pressures (densities), except for at 100 K for which measurements were only made

at two different pressures (see Table 1 for details). No effects were observed on the bimolecular rate coefficients as pressure, radical concentration, and probe wavelength were varied.

There have been several previous studies investigating the removal rates of $^1CH_2$ with various colliders. All those discussed in this section below employed a similar experimental technique (PLP-LIF) and detection scheme to that used in this study. For acetylene (R7) there have been two previous temperature dependent studies, by Blitz et al. (2000) and Gannon et al. (2010a). Both studies show a negative temperature dependence, however neither study has investigated removal rates below 195 K. Rate coefficients reported at room temperature in these two studies are in good agreement (within 15 %) with that reported in this study. However the value reported by Gannon et al. (2010a) at 195 K is around 25 % lower than the values reported in this study and by Blitz et al. (2000) (at 205 K). Taking the temperature dependent parameters quoted in these earlier studies and extrapolating the rate to 43 K, we find Gannon et al. (2010a) underestimates the rate by around 25 %, while Blitz et al. (2000) overestimates the rate by a factor of 2, highlighting the importance of experimental measurements at these low temperatures.

For ethylene (R8), there have been three previous temperature dependent studies, by Gannon et al. (2010a), Hayes et al. (1996), and Wagener (1990). All three studies show a negative temperature dependence, but again no study has investigated removal rates below 195 K. Rate coefficients determined in this work at 195 K and below are consistent with these higher temperature literature values. Using the temperature dependent parameters quoted in these studies to determine a rate coefficient at 43 K, we find that both Gannon et al. (2010a) and Wagener (1990) overestimate the rate by around 60 %, while the value from Hayes et al. (1996) puts the rate at over 200 times that determined in this study.

Hayes et al. (1996) and Wagener (1990) also reported temperature dependent removal rates for $^1CH_2$ with ethane (R9), with both reporting a negative temperature dependence. However, again neither study reports low temperature rates below 210 K. Using the temperature-dependent parameters reported in these two studies gives removal rates at 43 K that are, compared with the measurements in the present study, ~ 60 % faster for Wagener (1990) and over 700 times faster for the more recent study by Hayes et al. (1996). It should be noted that many Titan models use the extrapolated ethane rates reported by Hayes et al. (1996), which, even at temperatures more relevant to Titan's atmosphere (160 K), overestimate the removal determined experimentally in this study by a factor of 2.2.

For the reaction of $^3CH_2$ with O_2 (R19), there have been four room temperature values reported by Blitz et al. (2003), Darwin et al. (1989), Alvarez and Moore (1994) , and Hancock and Haverd (2003). The reaction was studied by Blitz et al. (2003) using a very similar procedure to that used in this work, while two of the other studies used laser flash photolysis of ketene at 351 nm to produce ground state $^3CH_2$, and monitored the reaction by detecting changes in the absorbance of either the $^3CH_2$ reactant (Darwin et al., 1989) or the CO product (Alvarez and Moore, 1994). Hancock and Haverd (2003) used time-resolved Fourier transform emission spectroscopy to monitor products from the reaction, with $^3CH_2$ also being produced by 351 nm photolysis of ketene. All four are, within experimental error,

in agreement with the room temperature value measured in this study. There has also been one previous temperature-dependent study by Bley et al. (1992), who used a discharge flow reactor with laser magnetic resonance detection of $^3CH_2$ and OH radicals, and electron spin resonance detection of O and H atoms. The positive temperature dependence reported by Bley et al. (1992) is inconsistent with the observations from this study which suggest a small negative temperature dependence. The room temperature rate coefficient reported by Bley et al. (1992) is also significantly lower (by ~ 60 %) than those reported in this and the other studies, and also has H atom yields which differ with the other literature; the disagreements in both kinetics and BR suggest that study may have been subject to unidentified systematic errors.

In combination with the literature values presented in Figure 6, the following T-dependant rate coefficient parameterizations are recommended for the removal of $^1CH_2$, and for the reaction of $^3CH_2$ with O_2:

$$k_{C_2H_2}(43 \leq T/K \leq 298) = (3.22 \pm 0.15) \times 10^{-10} \times (T/298)^{(-0.394 \pm 0.066)}$$

$$k_{C_2H_4}(43 \leq T/K \leq 298) = (2.16 \pm 0.14) \times 10^{-10} \times (T/298)^{(-0.612 \pm 0.089)}$$

$$k_{C_2H_6}(43 \leq T/K \leq 298) = (1.78 \pm 0.10) \times 10^{-10} \times (T/298)^{(-0.545 \pm 0.078)}$$

$$k_{^3CH_2 + O_2}(43 \leq T/K \leq 298) = (3.57 \pm 0.20) \times 10^{-12} \times (T/298)^{(-0.319 \pm 0.121)}$$

3.2. Branching Ratios

BRs for the reactive removal of $^1CH_2$ by, H_2, CH_4, C_2H_2, C_2H_4, and C_2H_6 determined in this study are presented in Figure 8 and Table 3 as a function of temperature, together with the available literature values. The BRs did not appear to be a function of pressure, radical concentration, or reagent concentrations, when these parameters were varied by up to a factor of 2.

For hydrogen, the BRs measured in this study are in good agreement with those measured in our previous study, and those reported in the literature by Gannon et al. (2008) and Blitz et al. (2001), both of whom used a very similar experimental technique and methodology to this study. Our current study does, however, suggest a more rapid decline in the reactive removal of $^1CH_2$ with decreasing temperature, falling to 17 % at 100 K rather than 22 % at 73 K.

The BRs measured for methane are also in good agreement with those measured in our previous study, and as reported at room temperature by Böhland et al. (1985), who employed laser magnetic resonance to directly measure the yields of $^3CH_2$ produced by intersystem crossing from $^1CH_2$.

For acetylene and ethylene, BRs were determined by comparing the yield of H atoms produced from reactions R7a and R8a to that of a calibration reaction, in this case the reaction of $^1CH_2$ with H_2 (R3a). These H atom yields were then converted into BRs using the BRs for H_2 determined in this current study. Gannon et al. (2010b) used a very similar experimental technique and methodology to report BRs for acetylene and ethylene down to

195 K, while in the same study as for methane above, Böhland et al. (1985) also reported a room temperature BR for ethylene. No studies have reported BRs below 195 K however. The room temperature BRs for reactive removal of acetylene and ethylene determined in this current study are in good agreement with the previous literature values. However disagreement we report a less rapid decline in reactive removal of $^1CH_2$ with decreasing temperature for both acetylene and ethylene than Gannon et al. (2010b), with our results suggesting chemical reaction of $^1CH_2$ with these species is still the dominant removal process at 160 K. This discrepancy is put down to systematic errors between the two studies. However, the general trend of the decreasing importance of reactive removal with decreasing temperature is apparent in both studies, with our results showing that reactive removal of $^1CH_2$ by acetylene and ethylene accounts for ≤ 15 % at 100 K.

There have been no previous temperature dependant studies on the BR for $^1CH_2$ with ethane, however Böhland et al. (1985) report a room temperature value which is in good agreement with that determined in this study. This study extends the temperature range of BRs down to 100 K, and shows that the fraction of $^1CH_2$ removed by chemical reaction decreases with decreasing temperature, falling to 56 % at 100 K.

In combination with the literature values presented in Figure 8, the temperature dependence of the branching ratios for reactive removal of $^1CH_2$ have been parameterized as follows:

$$BR_{(H_2)}\ (73 \leq T/K \leq 498) = (1.80 \pm 0.44) \times (T/298)^{(-0.42 \pm 0.29)} \times \exp^{((-210 \pm 69)/T)}$$

$$BR_{(CH_4)}\ (73 \leq T/K \leq 298) = (0.863 \pm 0.038) \times (T/298)^{(0.50 \pm 0.10)}$$

$$BR_{(C_2H_2)}\ (100 \leq T/K \leq 498) = (2.04 \pm 0.48) \times \exp^{((-264 \pm 60)/T)}$$

$$BR_{(C_2H_4)}\ (100 \leq T/K \leq 498) = (1.57 \pm 0.29) \times \exp^{((-199 \pm 46)/T)}$$

$$BR_{(C_2H_6)}\ (100 \leq T/K \leq 298) = (0.822 \pm 0.020) \times (T/298)^{(0.43 \pm 0.06)}$$

4. Discussion

4.1. Titan model

To understand the implications of the measured rate coefficients and BRs, the results have been included in a 1D transport model of Titan's atmosphere from Cal-tech/JPL (Allen et al., 1981; Yung, 1987; Yung et al., 1984; Zhang et al., 2010). The model contains the new set of chemical reactions from Moses et al. (2005), which was reviewed and updated with the most recent literature values (Douglas et al., 2018). The background atmospheric density and temperature profiles used in the model were constructed from Cassini observations, and the eddy diffusion coefficient taken from Li et al. (2014). Although the importance of ion-molecule reactions in Titan's atmosphere is well known (e.g. (Vuitton et al., 2008)), to reduce model complexity and to focus on the results of this study, only neutral hydrocarbons and nitriles are included.

As in our previous study, two model runs were conducted: the first a base case scenario in which the most up-to-date literature rate coefficients for the reactions of $^1CH_2$ with C_2H_2 (R7), C_2H_4 (R8), and C_2H_6 (R9) were used, while the second incorporated the low temperature rate coefficients and BRs measured in this study. The parameterized rate coefficients used in both model runs can be found in Table 4. For the base case scenario, for the reaction of $^1CH_2$ with C_2H_2, the parameterized rate coefficients given by Hebrard et al. (2013), which have been used in other recent models of Titan's atmosphere ((Dobrijevic et al., 2016; Loison et al., 2015)), were used. These parameterizations were based on the experimental data by Gannon et al. (2010b) and Gannon et al. (2010a). For the reaction of $^1CH_2$ with C_2H_4, the BR between reaction and relaxation determined by Gannon et al. (2010b) at 195 K was applied to the parameterized rate coefficient of (Gannon et al., 2010a), while for $^1CH_2$ with C_2H_6, the BR determined by Böhland et al. (1985) at 298 K was applied to the parameterized rate coefficient of Hayes et al. (1996).

Modelled vertical profiles obtained from both model runs for a selection of stable closed shell species are shown in Figure 9, together with observed mixing ratios. Modelled reaction rates, for the reactive removal of $^1CH_2$ by C_2H_2 (R7), C_2H_4 (R8), and C_2H_6 (R9) as a function of altitude are also presented in Figure 10. Whilst we are employing a simplified model omitting ion-molecule reactions, we are more interested in the relative changes in concentrations and reaction rates highlighted in this approach, rather than absolute values.

Moving from the base case scenario to this study, only minor changes (an increase or decrease of around 2 %) are observed in the mixing ratios of ethane, ethylene, and acetylene (Figure 9, only profiles using the new rates are shown for clarity), despite significant changes in the rates of R9a, R8a, and R7a (Figure 10). This is due to the fact that these reactions only account for a small fraction of the total loss processes of the reactants in these reactions. Similarly, the 60 % decrease in C_2H_5 and CH_3 from reaction R9a has little effect on the mixing ratios of stable products, as R9a accounted for only a small fraction (1.2 % for C_2H_5 and less than 0.1 % for CH_3) of the production of these species in the base scenario. The 100 % increase in H atoms produced via reactions R7a and R8a likewise have little effect on the mixing ratios of stable products, as both reactions account for less than 0.1 % of H atoms produced in the base scenario. The increase in production of the other products from reactions R8a (C_3H_5) and R7a (C_3H_3) does however affect the mixing ratios of several stable species. C_3H_5 production from reaction R8a increases by 60 %, resulting in an increase in the mixing ratio of $CH_3C{\equiv}CH$ of around 10 % at 800 km and upwards. This increase can be attributed to the direct formation of $CH_3C{\equiv}CH$ from the reaction of C_3H_5 with H atoms (R20), and moves the mixing ratios for this species to within error of those observed by the INMS at 1025 and 1077 km. C_3H_3 production from R7a increases by 140 %. As C_3H_3 recombination is one of the primary neutral routes to benzene formation (R10), a significant increase in the mixing ratio of C_6H_6 is observed throughout the atmosphere (Figure 9). This increase moves the modelled benzene concentrations closer to those observed by the INMS between 981 and 1077 km. Despite this, modelled concentrations remain around 2 orders of magnitude smaller than the observations. One possible explanation for this discrepancy could be an underestimation in the rate of one or more of the reactions forming benzene in our model, or even that an alternate neutral pathway to benzene exists that we do not account for.

A more likely explanation is the exclusion in our model of ion-molecule reactions that lead to benzene, as ion-molecule production rates of benzene have been shown to be significantly higher than neutral production rates of benzene above 700km (Vuitton et al., 2008). The increased production of C_3H_3 also results in higher concentration of other unsaturated hydrocarbons, namely 1-C_4H_6 and 1,2-C_4H_6, both of which see increases of around 20 % between 700 and 1550 km. Both these species are formed directly from the reaction of C_3H_3 with CH_3 (R21).

$$C_3H_5 + H \rightarrow CH_3C{\equiv}CH + H_2 \quad \text{(R20)}$$

$$C_3H_3 + CH_3 + M \rightarrow 1\text{-}C_4H_6 + M \quad \text{(R21a)}$$

$$C_3H_3 + CH_3 + M \rightarrow 1,2\text{-}C_4H_6 + M \quad \text{(R21b)}$$

In addition to observing significant changes in the rates of reactive removal of $^1CH_2$ by ethane, ethylene, and acetylene, we also observe significant changes in the rates at which these species electronically relax $^1CH_2$ down to ground state $^3CH_2$. When moving from the base case scenario to this study, we find that collision induced relaxation of $^1CH_2$ to $^3CH_2$ by ethane (R9b), ethylene (R8b), and acetylene (R7b) decreases by around 0.5 %, 45 %, and 27 %, respectively. Despite this, the total production rate of $^3CH_2$ remains largely unchanged, only dropping by 0.8 %, as the production of $^3CH_2$ from these channels only accounts for around 1.6 % of its total production rate. Looking at the total loss rate of $^1CH_2$ with these C_2H_x species, we again find little change, with the increase in reactive removal of $^1CH_2$ by ethylene and acetylene largely cancelling out the decrease in removal of $^1CH_2$ by electronic relaxation by the same species.

4.2. Implications

The importance of the reactions of $^1CH_2$ with C_2H_2, C_2H_4, and C_2H_6 to the atmosphere of Titan have been discussed in the Introduction. There are three important issues to consider in looking at the effect of these reactions on the concentrations of stable products: first, the loss of the stable C_2H_x species themselves via the reactive channels (R7a, R8a, and R9a); secondly, the production of new reactive radical species (also via the reactive channels) and their conversion to larger hydrocarbons such as benzene; and thirdly, the formation of ground state $^3CH_2$ via the electronic relaxation channels (R7b, R8b, and R9b) and its associated chemistry. As the model results indicate, the most significant of these effects is the formation of new radical species, while the destruction of the stable C_2H_x species and the production of $^3CH_2$ are likely to result in only minor changes. It should be noted, however, that these latter two issues may be of more consequence to other astrochemical environments, as discussed below.

Table 4 compares the rate coefficient expressions for the removal reactions of $^1CH_2$ with acetylene, ethylene, and ethane, as used in four recent chemical models of Titan's atmosphere. The rates given are for an altitude of 1000 km, at a temperature of 175 K and concentrations of C_2H_2 (3.9×10^6 molecule cm^{-3}), C_2H_4 (7.7×10^6 molecule cm^{-3}), and C_2H_6 (1.3×10^6 molecule cm^{-3}) as taken from Loison et al. (2015). No comparison with the models of Krasnopolsky (2014) and (Lara et al., 2014) could be made as these reactions were omitted

from their models. The chemical scheme of neutral species employed by Loison et al. (2015) has been used in a more recent paper by Dobrijevic et al. (2016) with only minor changes; the $^1CH_2$ chemistry has however remained unchanged.

As can be seen from Table 4, with the exception of the model by Vuitton et al. (2018), the majority of models of Titan's atmosphere employ temperature independent rate coefficients and BRs for the reactions of $^1CH_2$ with C_2H_2, C_2H_4, and C_2H_6, , where these reactions are included at all. Comparing the rates for the reactive removal of $^1CH_2$ by acetylene (R7a) to that determined in this study, it can be seen that the models by Vuitton et al. (2018) and Loison et al. (2015), and our base case model, significantly underestimate the rate by a factor of around 2.5, while the model of Lavvas et al. (2008) overestimates the rate by around 50 %. The rate of R7a used in the model of Willacy et al. (2016) is in good agreement with that determined in this study. As one of the products of this channel is C_3H_3, the primary precursor in the formation of benzene, it would be expected that models that underestimate this rate will underestimate the formation of benzene. Indeed when moving from our base case scenario to using the rates determined in this study, our model shows increased concentrations of benzene, which despite still being around 2 orders of magnitude smaller than those observed, does brings them into closer agreement. However, it should be noted that despite underestimating the rate of R7a, the model by Vuitton et al. (2018), which includes ion chemistry, predicts benzene concentrations in good agreement with observations. This highlights the importance of ion-molecule reactions to the production of benzene in the upper atmosphere of Titan. Indeed ion-molecule production rates of benzene have been shown to be significantly higher than the integrated neutral production rates (Vuitton et al., 2008).

Looking at the reactive removal rates of $^1CH_2$ by ethylene (R8a) to that determined in this study, the model by Loison et al. (2015) underestimates the rate by around a factor of 3, our base case model and that of Vuitton et al. (2018) underestimate the rate by around a factor of 1.5, while in the models by Willacy et al. (2016) and Lavvas et al. (2008) this reaction is omitted altogether. As one of the products of this channel, C_3H_5, is an important precursor in the formation of $CH_3C{\equiv}CH$, this may help explain the small underestimation in the concentrations of this species in the base case and Loison et al. (2015) models. Predicted CH_3C_2H concentrations are not given for the models by Vuitton et al. (2018), Willacy et al. (2016), and Lavvas et al. (2008). Comparing the rates of reactive removal of $^1CH_2$ by ethane (R9a) to that determined in this study, it can be seen that the models of Vuitton et al. (2018) and Loison et al. (2015) slightly overestimate the rate of R9a by around 30 %, while our base case model overestimates the rate by around a factor of 2. The model by Lavvas et al. (2008) underestimates the rate of R9a by around a factor of 3, while in the model by Willacy et al. (2016) the reaction is omitted altogether. As discussed above, as this reaction only accounts for a small percentage of the total formation rates of the products of this channel (C_2H_5 and CH_3), these differences in rates are likely to have little impact on the concentrations of stable species. The same conclusions are also reached when comparing the rates of electronic relaxation of $^1CH_2$ by the C_2H_x species to those determined in our study. These rates range from being between twice as fast to around 6 times slower, however as demonstrated above when comparing our two model outputs, as these reactions (R7b, R8b, and R9b) only account

for a small fraction of the total $^3CH_2$ formed, these changes have little effect on the concentrations of stable species.

As discussed in the Introduction, reactions of $^1CH_2$ with hydrocarbon species are important to a range of planetary and astrophysical environments with temperatures significantly lower than those on Titan. Our measurements of the removal rate of $^1CH_2$ with C_2H_2 and C_2H_4 confirm the enhancement of the rate coefficients with decreasing temperature, but crucially also confirm our earlier measurements (Gannon et al., 2010a; Gannon et al., 2010b) of the decreasing importance of the reactive component at lower temperatures. We also offer the first determination of the temperature dependence on the BR of $^1CH_2$ with C_2H_6, for which we observe the same trend of decreasing importance of the reactive component at lower temperatures; a trend we also reported for the reactions of $^1CH_2$ with H_2 and CH_4 in a previous publication (Douglas et al., 2018) and confirmed in our current work (Figure 8 and Table 3). For the reactions of $^1CH_2$ with C_2H_2 and C_2H_4, relaxation is the dominant channel at 100 K, accounting for 85 % and 86 % of the removal of $^1CH_2$ respectively. For the reaction of $^1CH_2$ with C_2H_6, relaxation has increased from 13 % at 298 K to 44 % at 100 K. To understand how these new experimentally determined rate coefficients and BRs may affect other low temperature environments, we compare the parameterized rate coefficients for the removal reactions of $^1CH_2$ with H_2, CH_4, C_2H_2, C_2H_4, and C_2H_6, as determined in this and our previous study, to those given in the Kinetic Database for Astrochemistry, KIDA (Wakelam et al., 2012). It should be noted that KIDA currently lists these rate coefficients as 'not rated', rather than as a 'recommended value', suggesting the reliability of the quoted rate coefficients is not known. As can be seen from Table 5, the total removal rates of $^1CH_2$ by all five species are significantly underestimated at 43 K using the KIDA rate coefficients, by around a factor of 2 for H_2 and C_2H_6, by around a factor of 4 for CH_4 and C_2H_4, and by almost a factor of 30 for C_2H_4. This underestimation is primarily due to the increasing importance of the relaxation channel that we observe at lower temperatures, with the KIDA rates for relaxation at 43 K being between 7 and 29 times lower than those of our rate coefficients. Looking at the rates of reactive removal of $^1CH_2$ by these species, we see good agreement (values within 30%) between the KIDA rates and ours for CH_4 and C_2H_6. However, for H_2 and C_2H_2, the reactive removal of $^1CH_2$ at 45 K is significantly overestimated using the KIDA rate coefficients, being around a factor of 10 and factor of 100 times faster respectively, than our rates. The reactive removal channel for $^1CH_2$ with C_2H_4 is no included in the KIDA database. From this comparison, it is clear that models of low temperature hydrocarbon rich environments employing the KIDA rate coefficients are likely to significantly overestimate the roles of the reactive channels of $^1CH_2$, while underestimating the production and further chemistry of ground state $^3CH_2$.

5. Summary

The rate coefficients for the reactions of $^1CH_2$ with C_2H_2, C_2H_4, and C_2H_6 have been measured in a pulsed Laval system between 43 and 134 K, and in a low flow reaction cell between 160 and 298 K. All rate coefficients demonstrate a negative temperature dependence. Temperature-dependent branching ratios for reactive removal of $^1CH_2$ vs

quenching to ground state $^3CH_2$ have also been measured down to a temperature 100 K, for all three colliders and for H_2 and CH_4. Our studies demonstrate that whilst the absolute magnitude of $^1CH_2$ removal is enhanced at reduced temperatures, the fraction of reactive removal decreases, with electronic removal to $^3CH_2$ becoming the dominant channel for H_2, C_2H_2, and C_2H_4 at 100 K. For the two saturated hydrocarbons CH_4 and C_2H_6, removal of $^1CH_2$ via electronic relaxation reaches around 45 % at 100 K, up from around 15 % at room temperature.

The impacts of these new measurements for the atmosphere of Titan have been investigated using a 1D chemistry and transport model. Increases in the rate of reactive removal of $^1CH_2$ by ethane and ethylene of around 240 % and 160 % at altitudes of 500 km and above, result in increased production of C_3H_3 and C_3H_5. The increased amounts of C_3H_3 result in increased amounts (by around 25 %) of benzene in the upper atmosphere, while the greater concentrations of C_3H_5 result in a 10 % increase in $CH_3C{\equiv}CH$ concentrations. The implications of these new measurements for other low temperature astrophysical environments have also been examined. Rate constants provided in the KIDA significantly overestimate the reactive removal of $^1CH_2$ at a low temperature of around 45 K, while significantly underestimating the relaxation down to ground state $^3CH_2$. This suggests models of hydrocarbon rich environments employing the KIDA rate coefficients are likely to significantly overestimate the roles of the reactive channels of $^1CH_2$, while underestimating the production and further chemistry of ground state $^3CH_2$.

6. Figures

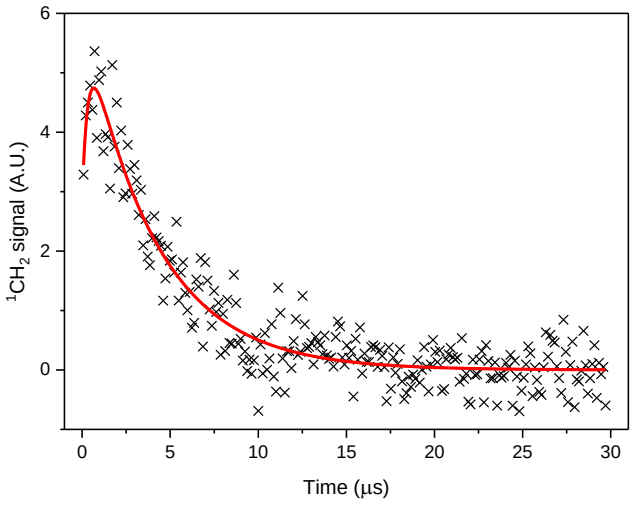

Fig. 1. Temporal evolution of the $^1CH_2$ LIF signal (black crosses) together with the nonlinear least-squares fit of eq (E1) to the data (solid red line) following 308 nm photolysis of ketene in the presence of $[C_2H_4] = 3.2 \times 10^{14}$ molecule cm^{-3} [total density $(1.0 \pm 0.2) \times 10^{17}$ molecule cm^{-3} in He, T = (43 ± 7) K, fit gives $k_{obs} = (249 \pm 11) \times 10^3$ s^{-1}].

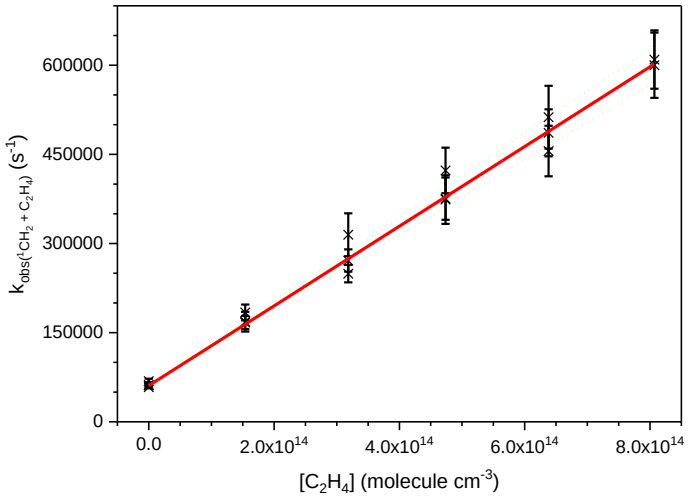

Fig. 2. Typical bimolecular plot for the removal of $^1CH_2$ with co-reactant, C_2H_4, at T = (43 ± 7) K, density = (1.0 ± 0.2) × 10^{17} molecule cm^{-3}, gradient gives $k_{(1CH2+H2)}$ = (6.70 ± 0.38) × 10^{-10} cm^3 $molecule^{-1}$ s^{-1}. The errors are statistical to the 2σ level.

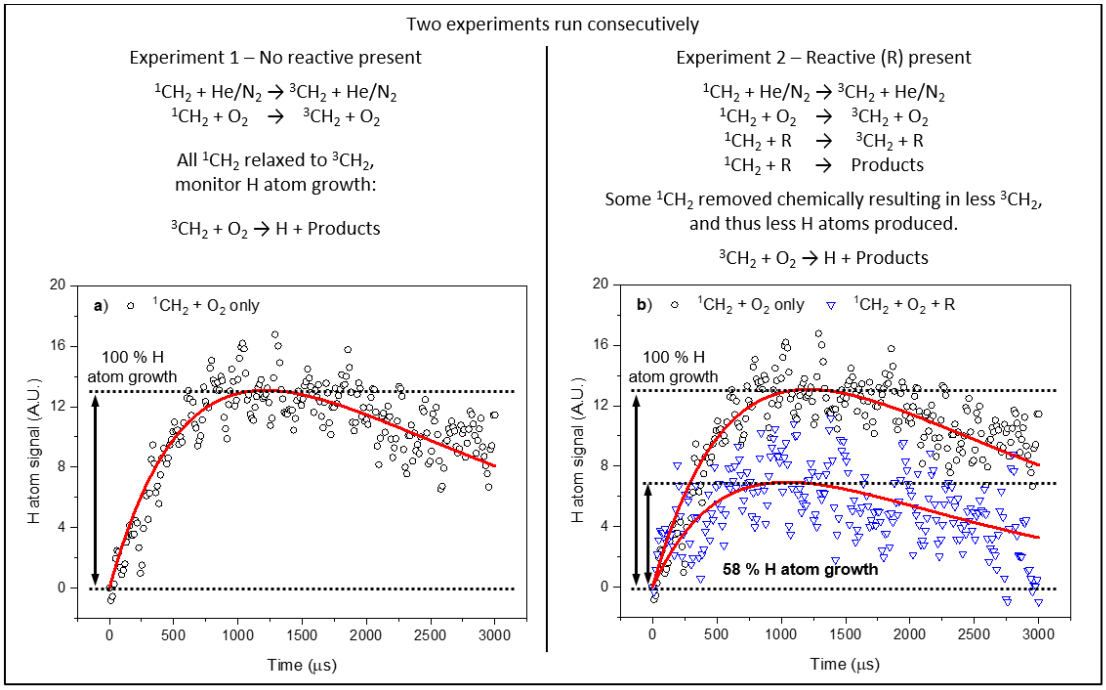

Fig. 3. Experimental scheme used to determine BRs for C_2H_6 by measuring H atom growth from the reaction of $^3CH_2$ with O_2. Traces show the temporal evolution of the H atom LIF signal (open symbols) together with the nonlinear least-squares fit of eq (E3) to the data (red solid lines) following 308 nm photolysis of ketene in the presence of a) [N_2] = 8.5 × 10^{16} molecule cm^{-3} and [O_2] = 8.2 × 10^{14}, and b) [N_2] = 3.2 × 10^{16} molecule cm^{-3}, [O_2] = 8.2 × 10^{14}, and [C_2H_6] = 1.8 × 10^{15} molecule cm^{-3}, at T = (160 ± 5 K). Panel b) has been

normalized for absorption of the Lyman-α radiation by C_2H_6. Fits to eq (E3) give a) $[^3CH_2]_0$ = (13.0 ± 0.9) A.U. and b) $[^3CH_2]_0$ = (7.3 ± 0.5) A.U., giving a ratio of $^3CH_2$ with and without C_2H_6 present of 0.58 ± 0.05.

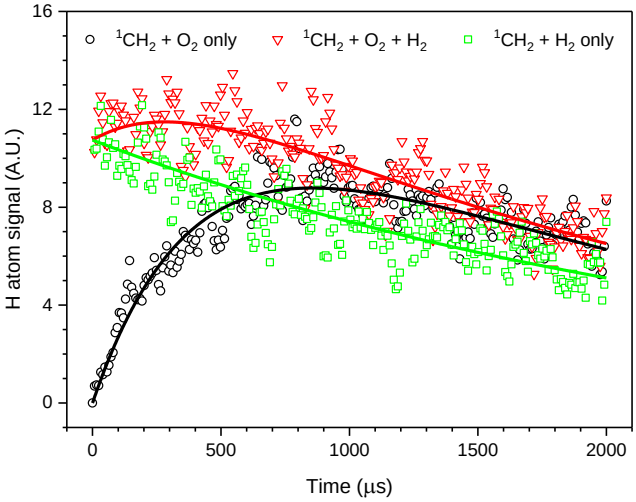

Fig. 4. The temporal evolution of the H atom LIF signals (open symbols) together with the nonlinear least-squares fit of Eq. E4 to the data (solid lines) following 308 nm photolysis of ketene in the presence of a) $[N_2] = 1.7 \times 10^{17}$ molecule cm^{-3} and $[O_2] = 8.5 \times 10^{14}$ molecule cm^{-3} (black circles), b) $[N_2] = 3.1 \times 10^{16}$ molecule cm^{-3}, $[O_2] = 8.5 \times 10^{14}$ molecule cm^{-3}, and $[H_2] = 1.4 \times 10^{17}$ molecule cm^{-3} (red triangles), and c) $[N_2] = 3.1 \times 10^{16}$ molecule cm^{-3}, and $[H_2] = 1.4 \times 10^{17}$ molecule cm^{-3} (green squares). T = (160 ± 5 K). In the fit for trace a) $[H]_0$ is set to zero, for trace c) $[^3CH_2]_0$ and k_{growth} are set to zero, and for trace b) $[H]_o$ is set to the value obtained from trace c). Fits to traces a) and b) give a ratio of $^3CH_2$ with and without H_2 present of 0.32 ± 0.05.

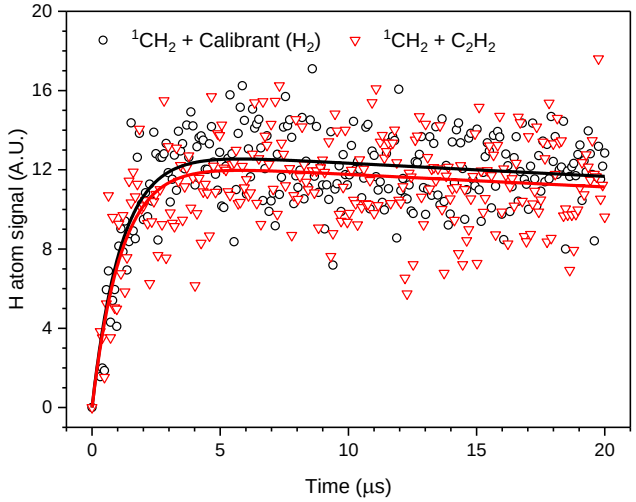

Fig. 5. Comparison of the H atom time profiles for the reaction of $^1CH_2$ with the calibrant gas H_2 (black circles, $[H_2] = 6.4 \times 10^{15}$ molecule cm^{-3}), and C_2H_2 (red triangles, $[C_2H_2 = 1.9 \times 10^{15}$ molecule cm^{-3}), together with the nonlinear least-squares fit of Eq. E5 to the data (solid lines) [total density $(1.5 \pm 0.4) \times 10^{17}$ molecule cm^{-3} in He, T = (100 ± 19) K]. Fits to Eq. E5 give an H atom yield of 0.93 ± 0.04 for the reaction of $^1CH_2$ with C_2H_2 compared to that of the calibration reaction.

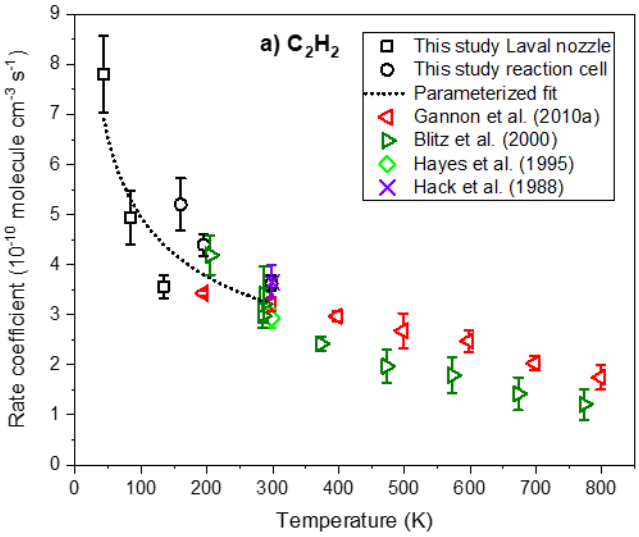
a) C_2H_2
This study Laval nozzle
This study reaction cell
Parameterized fit
Gannon et al. (2010a)
Blitz et al. (2000)
Hayes et al. (1995)
Hack et al. (1988)
Rate coefficient (10^{-10} molecule cm^{-3} s^{-1})
Temperature (K)

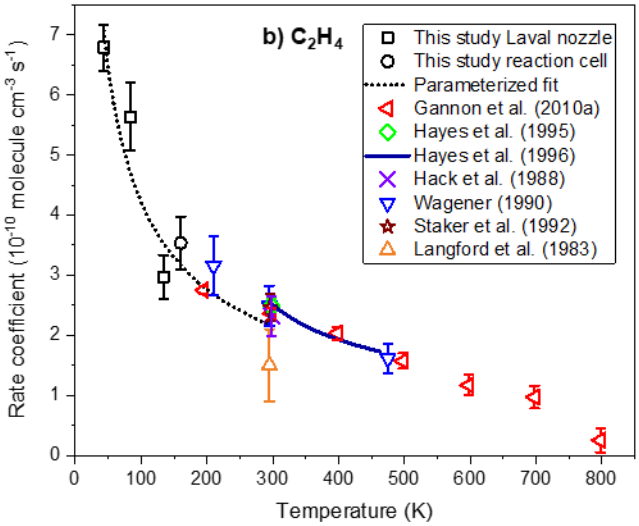
b) C_2H_4
This study Laval nozzle
This study reaction cell
Parameterized fit
Gannon et al. (2010a)
Hayes et al. (1995)
Hayes et al. (1996)
Hack et al. (1988)
Wagener (1990)
Staker et al. (1992)
Langford et al. (1983)
Rate coefficient (10^{-10} molecule cm^{-3} s^{-1})
Temperature (K)

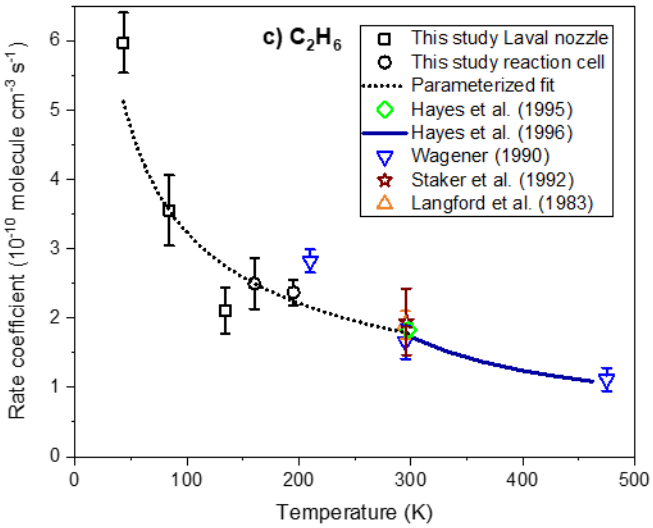
c) C_2H_6
This study Laval nozzle
This study reaction cell
Parameterized fit
Hayes et al. (1995)
Hayes et al. (1996)
Wagener (1990)
Staker et al. (1992)
Langford et al. (1983)
Rate coefficient (10^{-10} molecule cm^{-3} s^{-1})
Temperature (K)

705

Fig. 6. Temperature dependence of the rate coefficients for $^1CH_2$ + a) acetylene, b) ethylene, and c) ethane reported in this work and in the literature. Uncertainty ranges are given at 95 % confidence. Black open squares: this study Laval nozzle experiments. Black circles: this study reaction cell experiments. Red left facing triangles: (Gannon et al., 2010a). Dark green right facing triangles (Blitz et al., 2000) . Light green diamonds (Hayes et al., 1995). Purple crosses (Hack et al., 1988). Dark blue line: (Hayes et al., 1996). Blue downward triangles: (Wagener, 1990). Dark red stars (Staker et al., 1992). Orange upward triangles: (Langford et al., 1983). The black dotted lines are a parameterization of the data at 298 K and below.

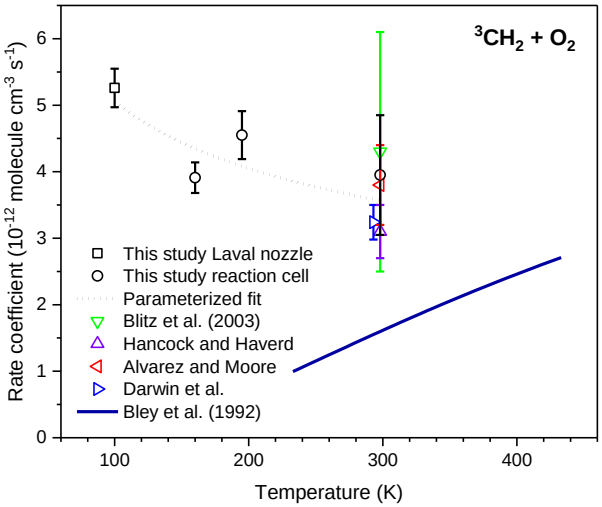

Fig 7. Temperature dependence of the rate coefficients for the reaction of $^3CH_2$ with O_2 reported in this work and in the literature. Uncertainty ranges are given at 95 % confidence. Black squares: this study Laval nozzle experiments. Black circles: this study reaction cell experiments. Green downward triangle: (Blitz et al., 2003). Purple upward triangle: (Hancock and Haverd, 2003). Red left facing triangle: (Alvarez and Moore, 1994). Blue right facing triangle: (Darwin et al., 1989). Dark blue solid line: (Bley et al., 1992). The black dotted line is a parameterization of the data at 298 K and below (excluding the data of Bley et al. (1992)).

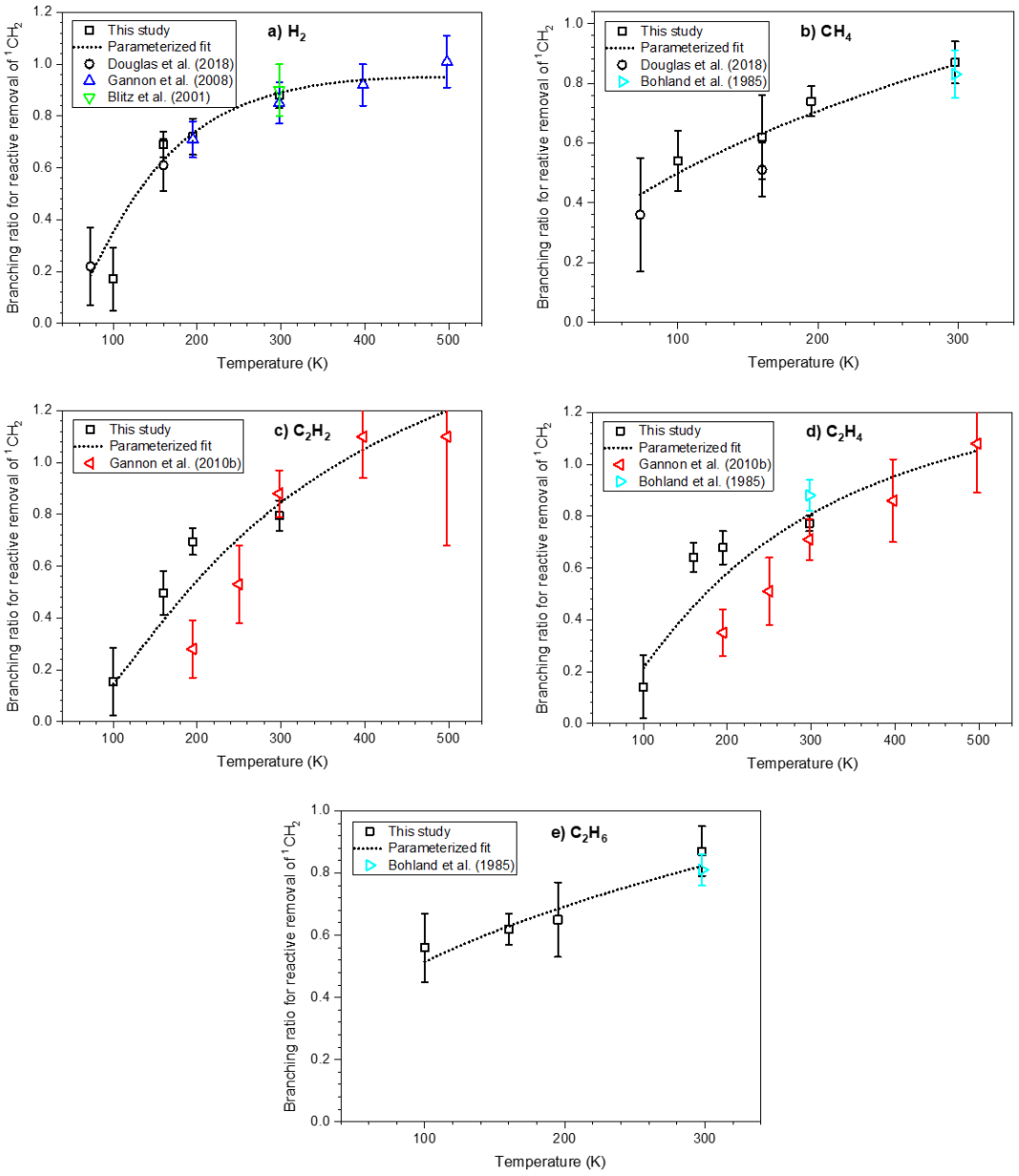

725

726 **Fig. 8.** Temperature dependence of the BR for reactive removal of $^1CH_2$ with a) H_2, b) CH_4,
727 c) C_2H_2, d) C_2H_4, and e) C_2H_6, reported in this work and in the literature. Uncertainty ranges
728 are given at 95 % confidence. Black squares: this study. Black circles: values from our earlier
729 study (Douglas et al., 2018). Blue upward triangles: (Gannon et al., 2008). Green downward
730 triangle: (Blitz et al., 2001). Turquoise right facing triangles: (Böhland et al., 1985). Red left
731 facing triangles: (Gannon et al., 2010b). The black dotted lines are a parameterization of the
732 combined data from this study and the literature values included in this figure.
733

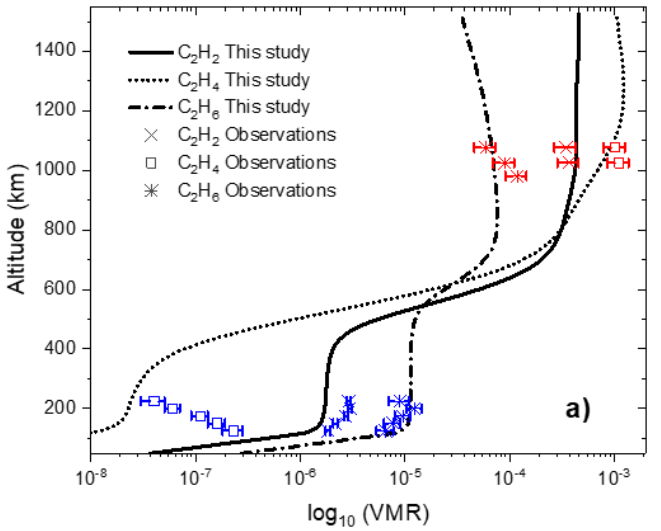
C_2H_2 This study
C_2H_4 This study
C_2H_6 This study
C_2H_2 Observations
C_2H_4 Observations
C_2H_6 Observations
Altitude (km)
$\log_{10}$ (VMR)
a)

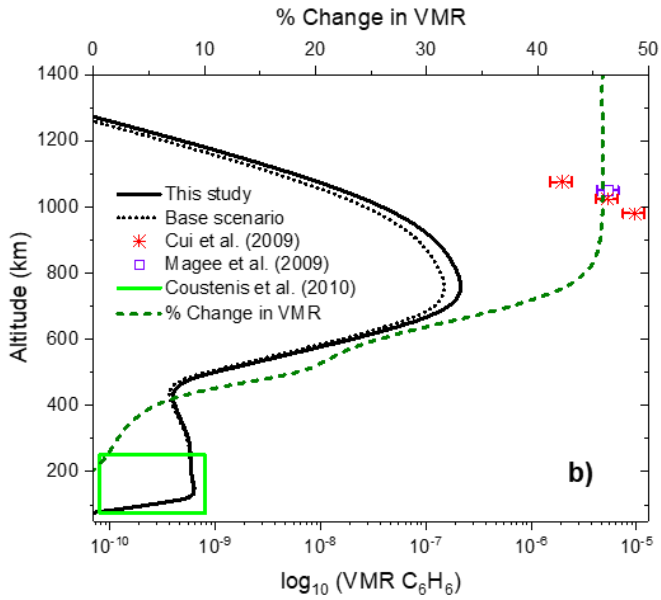
% Change in VMR
This study
Base scenario
Cui et al. (2009)
Magee et al. (2009)
Coustenis et al. (2010)
% Change in VMR
Altitude (km)
$\log_{10}$ (VMR C_6H_6)
b)

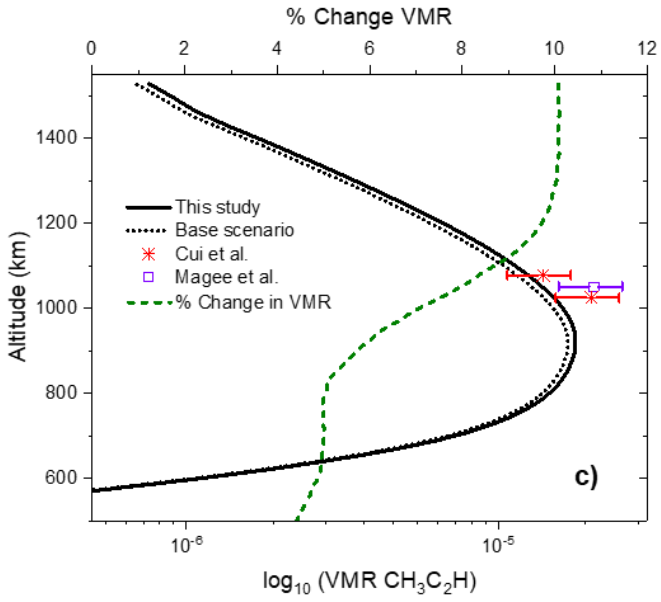
% Change VMR
This study
Base scenario
Cui et al.
Magee et al.
% Change in VMR
Altitude (km)
$\log_{10}$ (VMR CH_3C_2H)
c)

734

Fig. 9. Modelled vertical mixing ratio (VMR) profiles for both the base case scenario [dashed black lines in b) and c)] and using the rate coefficients determined in this study [all profiles in a) and solid black lines in b) and c)], and comparison with observations. The % change in VMR for C_6H_6 and $CH_3C{\equiv}CH$ on moving from the base scenario to this work is shown as a dark green dashed line in b) and c). Observations - Blue symbols: CIRS Limb (Nixon et al., 2013). Red symbols: INMS (Cui et al., 2009). Purple symbols: INMS (Magee et al., 2009). Green box: CIRS Nadir (Coustenis et al., 2010). A correction factor of 2.2 ± 0.5 has been applied to the INMS data (Teolis et al., 2015).

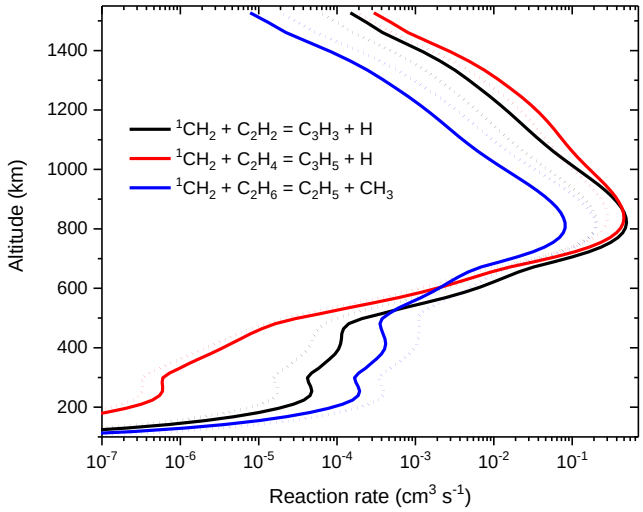

Fig. 10. A comparison of modelled reaction rates as a function of altitude, for the base case scenario (dashed lines) and using the rates determined in this study (solid lines).

7. Tables

Table 1. Characteristics of Laval nozzle gas expansions used in this study. [a] Range of conditions used in reaction cell experiments.

T (K)	Bath gas M	[M] (10^{16} molecule cm^{-3})
43 ± 7	He	5.5 ± 1.4 6.9 ± 2.1 8.1 ± 2.4 10.0 ± 2.0
84 ± 15	He	13.2 ± 3.2 18.4 ± 5.2 24.1 ± 7.0
100 ± 19	He	15.3 ± 4.1 20.7 ± 6.5
134 ± 21	N_2	3.2 ± 1.1 5.3 ± 2.0 10.0 ± 4.6
[a]160 ± 5	He or N_2	2.0 – 10.0 (± 5 %)

Table 2. Bimolecular rate constants for the removal of $^1CH_2$ with C_2H_2, C_2H_4, and C_2H_6, and for the reaction of $^3CH_2$ with O_2. Errors reported for the measurements made in this study are statistical at the 2σ level. Literature values taken from a) (Gannon et al., 2010a), b) (Hayes et al., 1995), and c) (Blitz et al., 2003).

	Rate coefficient k_r (cm^3 $molecule^{-1}$ s^{-1})			
T (K)	**$^1CH_2 + C_2H_2$ / 10^{-10}**	**$^1CH_2 + C_2H_4$ / 10^{-10}**	**$^1CH_2 + C_2H_6$ / 10^{-10}**	**$^3CH_2 + O_2$ / 10^{-12}**
43 ± 7	7.81 ± 0.77	6.79 ± 0.38	5.97 ± 0.43	
84 ± 15	4.94 ± 0.53	5.64 ± 0.56	3.55 ± 0.51	
100 ± 19				5.26 ± 0.29
134 ± 21	3.26 ± 0.23	2.83 ± 0.35	2.01 ± 0.31	
160 ± 5	5.20 ± 0.52	3.54 ± 0.44	2.50 ± 0.37	3.91 ± 0.23
195 ± 5	4.40 ± 0.22 3.43 ± 0.06[a]	2.75 ± 0.06[a]	2.36 ± 0.18	4.55 ± 0.36
298 ± 5	3.63 ± 0.16 3.21 ± 0.14[a]	2.36 ± 0.10[a]	1.83 ± 0.10[b]	3.95 ± 0.90 4.3 ± 1.8[c]

Table 3. Branching ratio for reactive removal of $^1CH_2$ with H_2, CH_4, C_2H_2, C_2H_4, and C_2H_6, as a function of temperature. Errors reported for the measurements made in this study represent statistical uncertainty (2σ) in the experimental data. Literature values taken from a) (Douglas et al., 2018), b) (Gannon et al., 2008), c) (Blitz et al., 2001), d) (Böhland et al., 1985), and e) (Gannon et al., 2010b).

T / K	**H_2**	**CH_4**	**C_2H_2**	**C_2H_4**	**C_2H_6**
73	0.22 ± 0.15[a]	0.36 ± 0.19[a]			
100	0.17 ± 0.12	0.54 ± 0.10	0.15 ± 0.07	0.14 ± 0.03	0.56 ± 0.11
160	0.69 ± 0.02 0.61 ± 0.10[a]	0.62 ± 0.14 0.51 ± 0.09[a]	0.50 ± 0.19	0.65 ± 0.08	0.62 ± 0.05
195	0.72 ± 0.07 0.71 ± 0.07[b]	0.74 ± 0.05	0.69 ± 0.09 0.28 ± 0.11[e]	0.68 ± 0.06 0.35 ± 0.09[e]	0.65 ± 0.15
250			0.53 ± 0.15[e]	0.51 ± 0.13[e]	
298	0.88 ± 0.02 0.85 ± 0.08[b] 0.90 ± 0.10[c]	0.87 ± 0.07 0.83 ± 0.08[d]	0.82 ± 0.11 0.88 ± 0.09[e]	0.79 ± 0.05 0.88 ± 0.06[d] 0.71 ± 0.08[e]	0.87 ± 0.08 0.81 ± 0.05[d]

Model		$^1CH_2+C_2H_2$ k(T)[a]	k(175 K)[a] (1000 × k'/s^{-1})	Ratio This work/Model	$^1CH_2+C_2H_4$ k(T)[a]	k(175 K)[a] (1000 × k'/s^{-1})	Ratio This work/Model	$^1CH_2+C_2H_6$ k(T)[a]	k(175 K)[a] (1000 × k'/s^{-1})	Ratio This work/Model
Vuitton et al. (2018)	Reaction	7.90×10^{-10}. $T^{-0.39}$	1.05×10^{-10} (0.41)	**2.18**	8.80×10^{-9}. $T^{-0.84}$	1.15×10^{-10} (0.88)	**1.74**	2.24×10^{-8}. $T^{-0.90}$	2.15×10^{-10} (0.28)	**0.72**
	Relaxation	2.03×10^{-9}. $T^{-0.39}$	2.71×10^{-10} (1.04)	**0.59**	1.63×10^{-8}. $T^{-0.84}$	2.13×10^{-10} (1.64)	**0.54**	3.60×10^{-11}	3.60×10^{-11} (0.05)	**2.31**
Willacy et al. (2016)	Reaction	2.50×10^{-10}	2.50×10^{-10} (0.96)	**0.92**	Not included	-	-	Not included	-	-
	Relaxation	6.60×10^{-11}	6.60×10^{-11} (0.25)	**2.41**	1.80×10^{-11}	1.80×10^{-11} (0.14)	**6.40**	3.60×10^{-11}	3.60×10^{-11} (0.05)	**2.31**
Loison et al. (2015) and Dobrijevic et al. (2016)	Reaction	7.60×10^{-11}. $(T/300)^{-0.30}$	8.93×10^{-11} (0.34)	**2.58**	6.30×10^{-11}	6.30×10^{-11} (0.48)	**3.17**	1.90×10^{-10}	1.90×10^{-10} (0.24)	**0.81**
	Relaxation	2.30×10^{-10}	2.30×10^{-10} (0.88)	**0.69**	1.40×10^{-10}	1.40×10^{-10} (1.08)	**0.82**	3.60×10^{-11}	3.60×10^{-11} (0.05)	**2.31**
Lavvas et al. (2008)	Reaction	3.27×10^{-10}	3.27×10^{-10} (1.26)	**0.70**	Not included	-	-	5.90×10^{-11}	5.90×10^{-11} (0.08)	**2.60**
	Relaxation	9.20×10^{-11}	9.20×10^{-11} (0.35)	**1.73**	2.30×10^{-11}	2.30×10^{-11} (0.18)	**5.01**	3.60×10^{-11}	3.60×10^{-11} (0.05)	**2.31**
Base case scenario	Reaction	7.6×10^{-11}. $(T/300)^{-0.30}$	8.93×10^{-11} (0.34)	**2.58**	7.40×10^{-11}. $(T/298)^{-0.84}$	1.16×10^{-10} (0.89)	**1.73**	3.73×10^{-11}. $e^{(-397/T)}$	3.61×10^{-10} (0.46)	**0.43**
	Relaxation	2.30×10^{-10}	2.30×10^{-10} (0.88)	**0.69**	1.37×10^{-10}. $(T/298)^{-0.84}$	2.14×10^{-10} (1.65)	**0.54**	8.74×10^{-12}. $e^{(-397/T)}$	8.45×10^{-11} (0.11)	**0.99**
This work	Reaction	1.75×10^{-9}. $(T/298)^{-2.18}$. $e^{(-558/T)}$	2.30×10^{-10} (0.89)	1.00	1.88×10^{-9}. $(T/298)^{-3.56}$. $e^{(-724/T)}$	2.00×10^{-10} (1.54)	1.00	1.48×10^{-10}. $(T/298)^{-0.171}$. $e^{(-9.57/T)}$	1.53×10^{-10} (0.20)	1.00
	Relaxation	8.21×10^{-11}. $(T/298)^{-2.39}$. $e^{(-107/T)}$	1.59×10^{-10} (0.61)	1.00	5.24×10^{-11}. $(T/298)^{-2.95}$. $e^{(-137/T)}$	1.15×10^{-10} (0.89)	1.00	4.82×10^{-11}. $(T/298)^{-1.43}$. $e^{(-37.6/T)}$	8.32×10^{-11} (0.11)	1.00

Table 4. Comparison of rate coefficient expressions for the removal reactions of $^1CH_2$ with C_2H_2, C_2H_4, and C_2H_6 (R7, R8, and R9) as used in five chemical models of Titan's atmosphere. k' gives the rate at a temperature of 175 K and an altitude of 1000 km, while Ratio This work / Model gives the ratio of the k' values from the rates determined in this study, to those from the other models. See text for details. [a] units cm^3 $molecule^{-1}$ s^{-1}.

Rate coefficients		$^1CH_2+C_2H_2$ k(T)[a]	k(43 K)[a]	Ratio this work/KIDA	$^1CH_2+C_2H_4$ k(T)[a]	k(43 K)[a]	Ratio this work/KIDA	$^1CH_2+C_2H_6$ k(T)[a]	k(43 K)[a]	Ratio this work/KIDA
KIDA database	Reaction	8.14×10^{-11}	8.14×10^{-11}	**0.003**	Not included	-	-	1.90×10^{-10}	1.90×10^{-10}	**0.87**
	Relaxation	9.62×10^{-11}	9.62×10^{-11}	**7.24**	2.30×10^{-11}	2.30×10^{-11}	**28.5**	3.60×10^{-11}	3.60×10^{-11}	**8.90**
	Total removal		1.78×10^{-10}	**3.93**		2.30×10^{-11}	**28.5**		2.26×10^{-10}	**2.15**
This work	Reaction	$1.75 \times 10^{-9}.(T/298)^{-2.18}.e^{(-558/T)}$	2.76×10^{-13}	1.00	$1.88 \times 10^{-9}.(T/298)^{-3.56}.e^{(-724/T)}$	9.01×10^{-14}	1.00	$1.48 \times 10^{-10}.(T/298)^{-0.171}.e^{(-9.57/T)}$	1.65×10^{-10}	1.00
	Relaxation	$8.21 \times 10^{-11}.(T/298)^{-2.39}.e^{(-107/T)}$	6.97×10^{-10}	1.00	$5.24 \times 10^{-11}.(T/298)^{-2.95}.e^{(-137/T)}$	6.54×10^{-10}	1.00	$4.82 \times 10^{-11}.(T/298)^{-1.43}.e^{(-37.6/T)}$	3.20×10^{-10}	1.00
	Total removal		6.97×10^{-10}	1.00		6.55×10^{-10}	1.00		4.85×10^{-10}	1.00

Rate coefficients		$^1CH_2+H_2$ k(T)[a]	k(43 K)[a]	Ratio this work/KIDA	$^1CH_2+CH_4$ k(T)[a]	k(43 K)[a]	Ratio this work/KIDA
KIDA database	Reaction	1.20×10^{-10}	1.20×10^{-10}	**0.11**	5.90×10^{-11}	5.90×10^{-11}	**1.27**
	Relaxation	1.26×10^{-11}	1.26×10^{-11}	**20.7**	1.20×10^{-11}	1.20×10^{-11}	**16.7**
	Total removal		1.33×10^{-10}	**2.07**		7.10×10^{-11}	**3.89**
Douglas et al. (2018)	Reaction	$1.42 \times 10^{-10}.(T/300)^{-0.193}.e^{(-118/T)}$	1.33×10^{-11}	1.00	$6.65 \times 10^{-11}.(T/300)^{-0.056}.e^{(0.6/T)}$	7.52×10^{-11}	1.00
	Relaxation	$2.53 \times 10^{-11}.(T/300)^{-2.17}.e^{(-126/T)}$	2.61×10^{-10}	1.00	$2.48 \times 10^{-11}.(T/300)^{-2.92}.e^{(-154/T)}$	2.01×10^{-10}	1.00
	Total removal		2.74×10^{-10}	1.00		2.76×10^{-10}	1.00

Table 5. Comparison of rate coefficient expressions given by the KIDA database (Wakelam et al., 2012) to those determined in this and a previous (Douglas et al., 2018) study, for the removal reactions of $^1CH_2$ with H_2, CH_4, C_2H_2, C_2H_4, and C_2H_6, (R3, R4, R7, R8, and R9), together with the rates at a temperature of 45 K. See text for details. [a] units cm^3 $molecule^{-1}$ s^{-1}.

762

Acknowledgements

This study was supported by funding from the UK Science and Technology Facilities Council (grant ST/L0006281/).

References

Allen, M., Yung, Y. L., Waters, J. W., 1981. Vertical transport and photochemistry in the terrestrial mesosphere and lower thermosphere (50-120 km). J. Geophys. Res. (Space Phys.). 86**,** 3617-3627.

Alvarez, R. A., Moore, C. B., 1994. Absolute yields of carbon monoxide, carbon dioxide, and formaldehyde from the reaction methylene(X^3B_1) + oxygen by IR diode laser flash kinetic spectroscopy. J. Phys. Chem. 98**,** 174-83.

Arendale, W. F., Fletcher, W. H., 1957. Infrared Spectra of Ketene and Deuteroketenes. J. Chem. Phys. 26**,** 793-797.

Bley, U., Temps, F., Wagner, H. G., Wolf, M., 1992. Investigations of the reaction between CH_2 $\tilde{X}\,^3B_1$ and O_2 in the temperature range 233 K ≤ T ≤ 433 K. Ber. Bunsenge. Phys. Chem. 96**,** 1043-1048.

Blitz, M. A., Beasley, M. S., Pilling, M. J., Robertson, S. H., 2000. Formation of the propargyl radical in the reaction of $^1CH_2$ and C_2H_2: experiment and modelling. Phys. Chem. Chem. Phys. 2**,** 805-812.

Blitz, M. A., Johnson, D. G., Pesa, M., Pilling, M. J., Robertson, S. H., Seakins, P. W., 1997. Reaction of CH radicals with methane isotopomers. J. Chem. Soc., Faraday Trans. 93**,** 1473-1479.

Blitz, M. A., McKee, K. W., Pilling, M. J., Seakins, P. W., 2003. Evidence for the dominance of collision-induced intersystem crossing in collisions of $^1CH_2$ with O_2 and a determination of the H atom yields from $^3CH_2$ +O_2, using time-resolved detection of H formation by vuvLIF. Chem. Phys. Lett. 372**,** 295-299.

Blitz, M. A., Pilling, M. J., Seakins, P. W., 2001. Collision induced intersystem crossing in methylene on reactive surfaces: application of a new technique to CH2(a^1A_1)+H_2. Phys. Chem. Chem. Phys. 3**,** 2241-2244.

Blitz, M. A., Seakins, P. W., 2012. Laboratory studies of photochemistry and gas phase radical reaction kinetics relevant to planetary atmospheres. Chem. Soc. Rev. 41**,** 6318-6347.

Böhland, T., Temps, F., Wagner, H. G., 1985. The contributions of intersystem crossing and reaction in the removal of CH_2($\tilde{a}^1A_1$) by hydrocarbons studied with the LMR. Ber. Bunsenge. Phys. Chem. 89**,** 1013-1018.

Brownsword, R. A., et al., 1997. Kinetics over a wide range of temperature (13-744 K): Rate constants for the reactions of CH(v=0) with H_2 and D_2 and for the removal of CH(v=1) by H_2 and D_2. J. Chem. Phys. 106**,** 7662-7677.

Canosa, A., Sims, I. R., Travers, D., Smith, I. W. M., Rowe, B. R., 1997. Reactions of the methylidine radical with CH_4, C_2H_2, C_2H_4, C_2H_6, and but-1-ene studied between 23 and 295 K with a CRESU apparatus. Astron. Astrophys. 323**,** 644-651.

Caravan, R. L., Shannon, R. J., Lewis, T., Blitz, M. A., Heard, D. E., 2015. Measurements of Rate Coefficients for Reactions of OH with Ethanol and Propan-2-ol at Very Low Temperatures. J. Phys. Chem. A. 119**,** 7130-7137.

Coustenis, A., et al., 2010. Titan trace gaseous composition from CIRS at the end of the Cassini–Huygens prime mission. Icarus. 207**,** 461-476.

Cui, J., et al., 2009. Analysis of Titan's neutral upper atmosphere from Cassini Ion Neutral Mass Spectrometer measurements. Icarus. 200**,** 581-615.

Darwin, D. C., Young, A. T., Johnston, H. S., Moore, C. B., 1989. Rate constants for $^3CH_2$ removal by O_2, NO and C_2H_2 from IRTDLS. J. Phys. Chem. 93**,** 1074-1078.

Dobrijevic, M., Loison, J. C., Hickson, K. M., Gronoff, G., 2016. 1D-coupled photochemical model of neutrals, cations and anions in the atmosphere of Titan. Icarus. 268**,** 313-339.

Douglas, K., et al., 2018. Low temperature studies of the removal reactions of (CH2)-C-1 with particular relevance to the atmosphere of Titan. Icarus. 303**,** 10-21.

Fisher, G. J., Maclean, A. F., Schnizer, A. W., 1953. Apparatus for the preparation of ketene by the pyrolysis of acetic anhydride. J. Org. Chem. 18**,** 1055-1057.

Gannon, K. L., Blitz, M. A., Liang, C. H., Pilling, M. J., Seakins, P. W., Glowacki, D. R., 2010a. Temperature Dependent Kinetics (195-798 K) and H Atom Yields (298-498 K) from Reactions of $^1CH_2$ with Acetylene, Ethene, and Propene. J. Phys. Chem. A. 114**,** 9413-9424.

Gannon, K. L., et al., 2010b. An experimental and theoretical investigation of the competition between chemical reaction and relaxation for the reactions of $^1CH_2$ with acetylene and ethene: implications for the chemistry of the giant planets. Faraday Discuss. 147**,** 173-188.

Gannon, K. L., Blitz, M. A., Pilling, M. J., Seakins, P. W., Klippenstein, S. J., Harding, L. B., 2008. Kinetics and product branching ratios of the reaction of $^1CH_2$ with H_2 and D_2. J. Phys. Chem. A. 112**,** 9575-9583.

Gans, B., et al., 2011. Photolysis of methane revisited at 121.6 nm and at 118.2 nm: quantum yields of the primary products, measured by mass spectrometry. Phys. Chem. Chem. Phys. 13**,** 8140-8152.

Gomez Martin, J. C., Caravan, R. L., Blitz, M. A., Heard, D. E., Plane, J. M. C., 2014. Low Temperature Kinetics of the CH_3OH + OH Reaction. J. Phys. Chem. A. 118**,** 2693-2701.

Hack, W., Koch, M., Wagner, H. G., Wilms, A., 1988. Direct determination of CH2(A^1A_1) removal rates by C_2H_2 and C_6H_6. Ber. Bunsenge. Phys. Chem. 92**,** 674-678.

Hancock, G., Haverd, V., 2003. A time-resolved FTIR emission study of the gas phase removal processes of $CH_2(X^3B_1)$ and $CH_2(a^1A_1)$ in collisions with O_2. Chem. Phys. Lett. 372**,** 288-294.

Hancock, G., Heal, M. R., 1992. Temperature dependences of CH_2 ($\tilde{a}^1A_1$) removal rates by Ar, NO, H_2, and CH_2CO in the range 295 - 859 K. J. Phys. Chem. 96**,** 10316-10322.

Hayes, F., Gutsche, G. J., Lawrance, W. D., Staker, W. S., King, K. D., 1995. Singlet methylene removal by saturated and unsaturated hydrocarbons. Combust. Flame. 100**,** 653-660.

Hayes, F., Lawrance, W. D., Staker, W. S., King, K. D., 1996. Temperature dependences of singlet methylene removal rates. J. Phys. Chem. 100**,** 11314-11318.

Hebrard, E., Dobrijevic, M., Benilan, Y., Raulin, F., 2007. Photochemical kinetics uncertainties in modeling Titan's atmosphere: First consequences. Plan. Space Sci. 55**,** 1470-1489.

Hebrard, E., Dobrijevic, M., Loison, J. C., Bergeat, A., Hickson, K. M., Caralp, F., 2013. Photochemistry of C3Hp hydrocarbons in Titan's stratosphere revisited. Astron. Astrophys. 552.

Jensen, P., Bunker, P. R., 1988. The potential surface and stretching frequencies of X^3B_1 methylene (CH_2) determined from experiment using the Morse osciallator-rigid bender internal dynamics Hamiltonian. J. Chem. Phys. 89**,** 1327-1332.

Krasnopolsky, V. A., 2014. Chemical composition of Titan's atmosphere and ionosphere: Observations and the photochemical model. Icarus. 236**,** 83-91.

Langford, A. O., Petek, H., Moore, C. B., 1983. Collisional removal of $CH_2(^1A_1)$: Absolute rate constants for atomic and molecular collisional partners at 295 K. J. Chem. Phys. 78**,** 6650-6659.

Lara, L. M., Lellouch, E., González, M., Moreno, R., Rengel, M., 2014. A time-dependent photochemical model for Titan’s atmosphere and the origin of H2O. Astron. Astrophys. 566**,** A143.

Lavvas, P. P., Coustenis, A., Vardavas, I. M., 2008. Coupling photochemistry with haze formation in Titan's atmosphere, part I: Model description. Plan. Space Sci. 56**,** 27-66.

Li, C., Zhang, X., Kammer, J. A., Liang, M. C., Shia, R. L., Yung, Y. L., 2014. A non-monotonic eddy diffusivity profile of Titan's atmosphere revealed by Cassini observations. Plan. Space Sci. 104**,** 48-58.

Loison, J. C., et al., 2015. The neutral photochemistry of nitriles, amines and imines in the atmosphere of Titan. Icarus. 247**,** 218-247.

Lorenz, R. D., 2014. Titan: Interior, surface, atmosphere, and space environment, edited by AU - I. Müller-Wodarg , AU - C. A. Griffith , AU - E. Lellouch , and AU - T. E. Cravens . Cambridge, UK: PB - Cambridge University Press , 2014, 474 p. $135, hardcover (ISBN #978-0521199926). Meteoritics & Planetary Science. 49**,** 1139-1140.

Magee, B. A., Waite, J. H., Mandt, K. E., Westlake, J., Bell, J., Gell, D. A., 2009. INMS-derived composition of Titan's upper atmosphere: Analysis methods and model comparison. Plan. Space Sci. 57**,** 1895-1916.

Mahon, R., McIlrath, T. J., Myerscough, V. P., Koopman, D. W., 1979. Third-harmonic generation in argon, krypton, and xenon: bandwidth limitations in the vicinty of Lyman-α. IEEE J. Quantum. Elecron. 15**,** 444-451.

Morgan, C. G., Drabbels, M., Wodtke, A. M., 1996. The correlated product state distribution of ketene photodissociation at 308 nm. J. Chem. Phys. 104**,** 7460-7474.

Moses, J. I., Fouchet, T., Bezard, B., Gladstone, G. R., Lellouch, E., Feuchtgruber, H., 2005. Photochemistry and diffusion in Jupiter's stratosphere: Constraints from ISO observations and comparisons with other giant planets. J. Geophys. Res. (Planets). 110.

Nixon, C. A., et al., 2013. Detection of propene in Titan's stratosphere. Astrophys. J. Lett. 776.

Romanzin, C., et al., 2005 Methane photochemistry: A brief review in the frame of a new experimental program of Titan's atmosphere simulations. In: M. Bernstein, R. NavarroGonzalez, R. Raulin, (Eds.), Space Life Sciences: Astrobiology: Steps toward Origin of Life and Titan before Cassini, pp. 258-267.

Rowe, B. R., Marquette, J. B., 1987. CRESU studies of ion molecule reactions. Int. J. Mass Spectrom. Ion Processes. 80**,** 239-254.

Shannon, R. J., Blitz, M. A., Goddard, A., Heard, D. E., 2013. Accelerated chemistry in the reaction between the hydroxyl radical and methanol at interstellar temperatures facilitated by tunnelling. Nature Chemistry. 5**,** 745-749.

Shannon, R. J., Taylor, S., Goddard, A., Blitz, M. A., Heard, D. E., 2010. Observation of a large negative temperature dependence for rate coefficients of reactions of OH with oxygenated volatile organic compounds studied at 86-112 K. Phys. Chem. Chem. Phys. 12**,** 13511-13514.

Sims, I. R., Smith, I. W. M., 1995. Gas-phase reactions and energy-transfer at very-low temperatures. Annu. Rev. Phys. Chem. 46**,** 109-137.

Smith, I. W. M., 2006. Reactions at very low temperatures: Gas kinetics at a new frontier. Angew. Chem. Int. Ed. 45**,** 2842-2861.

Smith, I. W. M., Sage, A. M., Donahue, N. M., Herbst, E., Quan, D., 2006. The temperature-dependence of rapid low temperature reactions: experiment, understanding and prediction. Faraday Discuss. 133**,** 137-156.

Staker, W. S., King, K. D., Gutsche, G. J., Lawrance, W. D., 1992. Direct measurement of singlet methylene removal rates by organic species containing the - O - and > C = O moieties. J. Chem. Soc., Faraday Trans. 88**,** 659-662.

Taylor, S. E., Goddard, A., Blitz, M. A., Cleary, P. A., Heard, D. E., 2008. Pulsed Laval nozzle study of the kinetics of OH with unsaturated hydrocarbons at very low temperatures. Phys. Chem. Chem. Phys. 10**,** 422-437.

Teolis, B. D., et al., 2015. A Revised Sensitivity Model for Cassini INMS: Results at Titan. Space Sci. Rev. 190**,** 47-84.

Thiesemann, H., MacNamara, J., Taatjes, C. A., 1997. Deuterium kinetic isotope effect and temperature dependence in the reactions of CH[^{2}Pi] with methane and acetylene. J. Phys. Chem. A. 101**,** 1881-1886.

Toublanc, D., Parisot, J. P., Brillet, J., Gautier, D., Raulin, F., McKay, C. P., 1995. Photochemical modeling of Titan's atmosphere. Icarus. 113**,** 2-26.

Vinatier, S., et al., 2018. Study of Titan's fall southern stratospheric polar cloud composition with Cassini/CIRS: Detection of benzene ice. Icarus. 310**,** 89-104.

Vuitton, V., Yelle, R. V., Cui, J., 2008. Formation and distribution of benzene on Titan. Journal of Geophysical Research: Planets (1991–2012). 113.

Vuitton, V., Yelle, R. V., Klippenstein, S. J., Hörst, S. M., Lavvas, P., 2018. Simulating the density of organic species in the atmosphere of Titan with a coupled ion-neutral photochemical model. Icarus.

933 Wade, E. A., Clauberg, H., Kim, S. K., Mellinger, A., Moore, C. B., 1997. Dynamics of
934 rotational energy release for dissociation of singlet ketene and the singlet/triplet
935 branching ratio. J. Phys. Chem. A. 101**,** 732-739.

936 Wagener, R., 1990. Influence of the temperature on the removal rates of $CH_2(a^1A_1)$ by inter-
937 gases and hydrocarbons. Z. Naturforsch. A. 45**,** 649-656.

938 Wakelam, V., et al., 2012. A Kinetic Database for Astrochemistry (KIDA). Astrophys. J.
939 Supp. Ser. 199.

940 Willacy, K., Allen, M., Yung, Y., 2016. A new astrobiological model of the atmosphere of
941 Titan. Astrophys. J. 829**,** 11.

942 Wilson, E. H., Atreya, S. K., 2003. Chemical sources of haze formation in Titan's
943 atmosphere. Plan. Space Sci. 51**,** 1017-1033.

944 Wilson, E. H., Atreya, S. K., 2004. Current state of modeling the photochemistry of Titan's
945 mutually dependent atmosphere and ionosphere. J. Geophys. Res. (Planets). 109.

946 Yoon, Y. H., Hörst, S. M., Hicks, R. K., Li, R., de Gouw, J. A., Tolbert, M. A., 2014. The
947 role of benzene photolysis in Titan haze formation. Icarus. 233**,** 233-241.

948 Yung, Y. L., 1987. An update of nitrile photochemistry on Titan. Icarus. 72**,** 468-472.

949 Yung, Y. L., Allen, M., Pinto, J. P., 1984. Photochemisty of the atmosphere of Titan -
950 comparison between model and observations. Astrophys. J. Supp. Ser. 55**,** 465-506.

951 Zhang, X., Ajello, J. M., Yung, Y. L., 2010. Atomic carbon in the upper atmosphere of Titan.
952 Astrophys. J. Lett. 708**,** L18-L21.

953